Molecular Tracking and Cultivation Reveal Ammonia-Oxidizing Archaea as Emerging Commensals of the Human Skin Microbiome

Alexander Mahnert*[,1], Maximilian Dreer*[,2], Ülkü Perier[2], Michael Melcher[2], Stefanie Duller[1], Adina Lehnen[1], Theodora Goessler[1], Daniela Brunner[1], Thomas Graier[3], Peter Wolf[3], Rafael I. Ponce-Toledo[2,#], Logan H. Hodgskiss[2], Melina Kerou[+,2], Christine Moissl-Eichinger[+,1,4], and Christa Schleper[+,2]

* Shared authorship

[+] Shared corresponding authorship

[1] Medical University of Graz, D&R Institute for Hygiene, Microbiology, and Environmental Medicine, Graz, Austria

[2] University of Vienna, Archaea Biology and Ecogenomics Unit, Vienna, Austria

[3] Medical University of Graz, Department of Dermatology and Venereology, Graz, Austria

[4] BioTechMed Graz, Graz, Austria

[#] Present address: Institut de Systématique, Evolution et Biodiversité (ISYEB), Sorbonne Université, CNRS, Muséum National d'Histoire Naturelle, Paris, France

AM: alexander.mahnert@medunigraz.at

MD: maximilian.dreer@univie.ac.at

UP: uelkue.perier@univie.ac.at

MM: michael.melcher@univie.ac.at

SD: stefanie.duller@medunigraz.at

AL: adina.lehnen@outlook.de

TG: evo1822@gmx.net

DB: Brunner-da@web.de

TG: thomas.graier@medunigraz.at

PW: peter.wolf@medunigraz.at

RP: rafael-isaac.ponce_toledo@sorbonne-universite.fr

LH: logan.hodgskiss@univie.ac.at

MK: melina.kerou@univie.ac.at

CME: christine.moissl-eichinger@medunigraz.at

CS: christa.schleper@univie.ac.at

Abstract

Background: Ammonia-oxidizing archaea (AOA) have repeatedly been detected on human skin, yet their persistence, physiological traits, and adaptations remain poorly understood. Here, we identify *Nitrosocosmicus* species as integral members of the healthy skin microbiome using two complementary approaches.

Results: Through cultivation, we enriched two autotrophic strains, *Candidatus Nitrosocosmicus epidermidis* and *Ca. Nitrosocosmicus unguis*, from human skin samples. Genomic analyses revealed specific adaptations for skin colonization, including genomic islands and expanded gene families linked to interactions with host proteins and signaling pathways, distinguishing these AOA from their soil-dwelling relatives.

Parallel molecular profiling in cross-sectional and longitudinal cohorts (n=47) consistently detected *Nitrosocosmicus* particularly in sebaceous areas. Co-occurrence patterns with specific bacterial taxa reinforce their role as stable components of the skin microbiome.

Conclusions: These findings indicate that *Nitrosocosmicus* species are emerging commensals, evolutionarily capable of transitioning from soil to human skin, where they likely play a critical role in the skin ecosystem.

Keywords: Ammonia-oxidizing Archaea, skin microbiome, enrichments, comparative genomics, next generation sequencing, marker gene analysis, metagenomics, microscopy, quantitative PCR,

Background

The human body is an ecosystem populated by spatially organized microbial communities composed of bacteria, archaea, viruses/ phages and small eukaryotes, with diverse metabolic activities and interactions: the microbiome(Berg et al., 2020). In recent years, numerous studies have led to a better understanding of the mechanisms involved in the complex interplay between the host and its commensals and have revealed the fundamental role of the human microbiome in health and disease (Fan and Pedersen, 2020; Flowers and Grice, 2020; Gomaa, 2020). However, most studies on human microbial communities have focused exclusively on the bacterial microbiome, while other integral components, such as eukaryotes/fungi, archaea and viruses have remained largely overlooked (Bang and Schmitz, 2015; Borrel et al., 2020; Fan et al., 2023; Gaci et al., 2014; Nayfach et al., 2021). A systematic metagenomic study has recently revealed the extent of diversity and abundance of archaea in the human gut microbiome (Chibani et al., 2022), where the increased presence of methanogenic archaea affects short-chain fatty acid production and the overall host physiology (Kumpitsch et al., 2021).

The skin microbiome is similarly complex and harbors various bacterial species, including *Staphylococcus, Streptococcus, Corynebacterium, and Propionibacterium* (now *Cutibacterium*), and fungi such as *Malassezia* (Grice and Segre, 2011; Kong, 2011). The composition and diversity of the microbiome varies across different body sites (e.g. oily versus dry skin) and between individuals (Oh et al., 2016). As in the gut, microorganisms play essential roles in maintaining skin health as they provide protection against pathogens by

81 competing for nutrients and space, producing antimicrobial compounds and modulating the
82 skin's immune response (Byrd et al., 2018; Ross et al., 2017).
83 Human skin is also colonized by archaea (Moissl-Eichinger et al., 2017; Probst et al., 2013),
84 in particular by representatives of the ammonia oxidizing archaea (AOA), formerly
85 Thaumarchaeota, now class Nitrososphaeria and phylum Thermoproteota (Parks et al., 2022,
86 2020; Rinke et al., 2021). Although rather rare in abundance, archaeal signals were found in
87 human subjects analyzed by 16S rRNA gene sequencing and detection of archaeal *amoA*,
88 the gene for subunit A of the key enzyme ammonia monooxygenase used for ammonia
89 oxidation (Probst et al., 2013). AOA signatures were detected on all human subjects and were
90 closely related to those found earlier in cleanrooms and intensive care units (Moissl-Eichinger,
91 2011). Their presence was confirmed by fluorescence *in situ* hybridization (Probst et al., 2013),
92 454 pyro-sequencing (Moissl-Eichinger et al., 2017), and infrared hyperspectral imaging
93 (Moissl-Eichinger et al., 2017). Although the physiological relevance of AOA to the skin is still
94 subject to speculation, its potential role is intriguing considering that urea and ammonia are
95 components of human sweat and are the main energy sources of ammonia oxidizers. Also,
96 nitric oxide (NO), an important signaling molecule involved in diverse processes in humans, is
97 a byproduct of the ammonia oxidation process (Jessica A. Kozlowski et al., 2016).
98 Detection of archaea in human microbiomes is generally hampered by numerous
99 methodological obstacles, such as challenging cultivation (Alves et al., 2019; Klein et al., 2022;
100 Sun et al., 2019) and molecular detection issues (summarized in (Mahnert et al., 2018)),
101 because of the bacteria-centric orientation in sampling, cell lysis, DNA extraction protocols,
102 PCR primers, and classification databases. Consequently, archaeal signals often remain close
103 to or below the detection limit, making it difficult to understand the role of archaea on human
104 skin (Umbach et al., 2021). Such obstacles and the lack of cultivated strains of skin AOA have
105 left many questions unanswered, with respect to i) abundance, ii) longitudinal stability, iii)
106 association with human health, iv) physiology and metabolism, v) interaction with the bacterial
107 microbiome, and vi) specific adaptations to the human skin.

108 In this manuscript, we present the results of two complementary, but independent approaches
109 designed to investigate the persistence and characteristics of AOA on human skin: extensive
110 cultivation efforts and molecular analyses targeting AOA in both healthy and diseased
111 individuals.
112 These efforts yielded stable, highly enriched cultures of strains affiliated with the genus
113 *Candidatus* Nitrosocosmicus from human skin. Their genomes reveal features that could
114 facilitate colonization of the skin environment, but also highlight the genomic repertoire shared
115 among all members of the genus *Ca*. Nitrosocosmicus, a widespread environmental group of
116 AOA. Molecular profiling further tracked *Ca.* Nitrosocosmicus signatures across cohorts of
117 healthy volunteers and patients, identifying correlations with physical parameters and bacterial
118 co-occurrence patterns.
119 Together, these findings suggest that specific *Ca.* Nitrosocosmicus species or clades have
120 evolved distinct traits potentially enabling their transition from soil to specialized niches on
121 human skin, supported by genomic adaptations and their stable integration into the skin
122 microbiome.
123

124 ## Methods

125

126 **Initial cultivation**

127 Prior to enrichment setups, subjects not working in an experimental laboratory were pre-
128 screened for the presence of *Nitrososphaerales* by targeted 16S rRNA gene amplification. We
129 used 3 different primer pairs, two of which targeted 16S rRNA (Cren 771F/957R (Ochsenreiter
130 et al., 2003) and Arch 109F/1492R (Großkopf et al., 1998; Nicol et al., 2008) and one targeted
131 the *amoA* gene (19F/629R, (Arce et al., 2018; Pester et al., 2012)). In dilution tests with
132 template DNA primers Arch 109F/1492R turned out to be the most sensitive and were thus
133 used to screen individuals for the presence of AOA. All tested individuals (n=41) were positive
134 for AOA. In a first round of cultivation attempts diverse swabs and brushes were tested to

135 identify tools that are compatible with AOA growth. Sterile polyurethane single sponge swabs
136 (BD BBL™ CultureSwab™ EZ, Becton Dickinson, USA) were identified as most suitable for
137 enrichments, since they promoted growth of *Nitrososphaera viennensis* in pre-tests, while
138 several other materials turned out to be inhibitory for growth.
139 For enrichment cultures, sterile swabs premoistened with sterile freshwater medium (FWM
140 (De La Torre et al., 2008; Tourna et al., 2011)) were used to sequentially rub the face, neck,
141 upper body, back, arms, and legs to obtain as much biomass as possible. All following
142 procedures were performed under sterile conditions (laminar flow). The polyurethane swab
143 was removed from the plastic shaft and directly added to FWM (Enrichments T1S, X2B and
144 Z3A). For enrichment of R2S, free edges of a subjects' fingernails (two to three clippings each
145 obtained with a sterilized scissor) were directly added to FWM (Enrichment R). Earlier studies
146 had shown the suitability to use fingernail microbiomes to assess the skin microbiome, due to
147 scratching (Rayan and Flournoy, 1987).
148 All initial enrichments were set up in sterile 30 ml polystyrene screw cap tubes (Greiner)
149 containing 20 ml FWM supplemented with 0.5 mM NH4Cl, 20 µl non-chelated trace element
150 solution, 7.5 µM FeNaEDTA, 20 µl vitamin solution as well as 25 µg/ml carbenicillin and 25
151 µg/ml kanamycin (for detailed medium composition see table 1 in (Reyes et al., 2020; Tourna
152 et al., 2011)).
153 Variations between initial enrichments included the carbon source (2 mM Na_2CO_3 or $NaHCO_3$),
154 pH (7 or 8.5), temperature (28°C or 32°C) supplementation with organic substrates (0.5 mM
155 acetate and 0.5 mM pyruvate or none) and filter sterilized spent growth medium of
156 *Nitrososphaera viennensis* EN76 (Tourna et al., 2011) and *Ca.* Nitrosocosmicus
157 franklandianus C13 (Lehtovirta-Morley et al., 2016) (2.5% (v/v) (Supplementary Table S1).
158 Cultures were incubated aerobically for up to several months without shaking and in the dark.
159 First transfer of cultures was performed after 3 months and *amoA* sequences and 16S rRNA
160 gene sequences were determined for the initial enrichments that showed nitrite production as
161 well as for their first transfers (see Supplementary Table S2). The sequences were identical
162 in the original cultures and the corresponding transfer. For T1S enrichments 6 different donors

163 were sampled and 12 cultures (2 different growth conditions varying in organic acid addition)
164 were set up. Out of 12 enrichments one culture (and its subculture) was positive for ammonia
165 oxidation and after further passages yielded T1S. In the case of R2S, one culture out of 10
166 setups (2 donor individuals) was positive. For the enrichments of X2B and Z3A three
167 individuals were sampled and 6 initial setups yielded two positive cultures after 2 and 2.5
168 months respectively. Sequences of 16S rRNA and *amoA* showed only few point mutations to
169 the sequences of *Ca.* N. epidermidis.
170 Positive enrichments were routinely transferred (transfer volume 20% v/v) upon reaching
171 nitrite concentrations of approximately 450 µM. After transferring subcultures R2S and T1S
172 into a medium containing 10 µg/ml chloramphenicol, 10 µg/ml novobiocin and 10 µg/ml
173 streptomycin twice, no bacterial contaminants were detected, leaving the cultures with yeast
174 contaminants. Both Bacteria and fungi signatures were found in X2B and Z3A.
175
176 **Routine culture maintenance**
177 Enrichments were routinely cultivated in sterile 30 ml polystyrene screw cap tubes containing
178 18 ml FWM supplemented with 0.6 mM NH_4Cl, 2 mM Na_2CO_3 (R) or $NaHCO_3$ (T1S, X2B, or
179 Z3A), 20 µl non-chelated trace element solution without molybdenum ($Na_2MoO_4 \cdot 2H_2O$), 7.5
180 µM FeNaEDTA, 20 µl vitamin solution as well as 25 µg/ml carbenicillin and kanamycin and
181 were transferred every two to four weeks upon reaching nitrite concentrations of approximately
182 450 µM. The inoculation volumes were decreased to 10% (v/v).
183 The medium of enrichment R2S additionally contained 10 mM MOPS ((3-(N-morpholino)
184 propanesulfonic acid), titrated to pH 7 with HCl) and had a final pH of 7. Ammonium and nitrite
185 concentrations were measured colorimetrically by the indophenol method and Griess reagent
186 respectively, as described previously (Reyes et al., 2020; Tourna et al., 2011). Aliquots used
187 for ammonium measurements were frozen at -20°C and measured jointly at a later time point.
188 Cultures were incubated aerobically at 28°C without shaking in the dark. Solutions were
189 autoclaved (FWM, NH_4Cl) or filter sterilized with a 0.2 µm filter (trace element solution, vitamin
190 solution, FeNaEDTA, antibiotics) prior to use (Supplementary Fig. 1: Enrichment Scheme).

191

192 **Microscopy**

193 Cultures were 10x concentrated before being imaged with phase contrast light microscopy
194 using 60x and 100x oil immersion objectives. F_{420} autofluorescence was imaged using an F420
195 filter cube. For scanning electron microscopy six ml of each enrichment at late exponential
196 phase were concentrated by centrifugation (21000 g, 4°C, 30 min). Pellets were fixed in 2.5%
197 glutaraldehyde for 2 h, washed three times with 1x PBS and resuspended in 100 µl 1x PBS.
198 50 µl of the fixed cell suspension were spotted onto 0.01% poly-L-Lysine coated glass slides
199 (5 mm) and sedimented for 2 h, before being dehydrated in an ethanol series (30-100%, 5 min
200 each). The dehydrated cells were critical point dried in liquid carbon dioxide and subsequently
201 coated with gold in a sputter coater. Samples were imaged in a JEOL IT 300 scanning electron
202 microscope at 20 kV (CIUS imaging facility, Univ. of Vienna).

203

204 **DNA extraction of cultures**

205 High molecular weight (HMW) DNA of enrichment cultures was extracted by a combination of
206 chemical lysis based on a modified lysis buffer for *Sulfolobus acidocaldarius* (Meulenbroek et
207 al., 2013) and freeze-thawing, followed by a phenol chloroform extraction.
208 Between 0.3 to 0.5 L of each skin enrichment culture were concentrated by filtration (0.22 µm
209 MF-Millipore™ mixed cellulose ester (MCE) membrane filter), washed off the filter with FWM
210 and pelleted by centrifugation (21000 g, 4°C, 30 min). Pellets were resuspended in a modified
211 TENST buffer (20 mM Tris pH 8, 1 mM EDTA, 100 mM NaCl, 5% N-Lauroylsarcosine, 0.12%
212 Triton X-100) and incubated at 50°C for 1-2 hours. Samples were subsequently subjected to
213 three rounds of freeze-thawing (5 min at -70°C followed by 5 min at 70°C). Proteinase K was
214 added to a final concentration of 100 µg/ml and samples were incubated at 65°C for 1-2 hours.
215 After lysis HMW DNA was extracted by a standard phenol chloroform extraction (2x
216 Phenol:Chloroform:Isoamylalcohol 25:24:1, 2x Chloroform:Isoamylalcohol 24:1) with low-
217 speed centrifugation (4500 g, 4°C, 3 min) between steps. DNA was precipitated overnight at
218 4°C by adding 1µl glycogen as a carrier and 2x volume of a PEG6000 solution (30% PEG6000

219 (v/v), 1.6 M NaCl). The precipitated DNA was washed twice with 4°C cold 70% EtOH, air-dried
220 at room temperature for 15-30 min, resuspended in 50-60°C nuclease free water followed by
221 an incubation at 55°C for up to two hours. The extracted HMW DNA was quantified
222 fluorometrically with a Qubit™ 2.0 Fluorometer (Invitrogen) and stored at -20°C.
223
224 **Quantitative PCR**
225 Archaeal *amo*A genes were quantified in triplicate using primers *amoA*19F and *amoA*629R as
226 previously (Abby et al., 2018; Alves et al., 2019) with some modifications: 20 µl reactions
227 contained 10 µl Luna® Universal qPCR Master Mix, 3 µl nuclease free water, 0.5 µm of each
228 primer and 5 µl DNA template. DNA was amplified in a CFX Real Time PCR System (Bio-
229 Rad) with following cycling parameters: 95°C for 1 min, 40x cycles of 95°C 15 s denaturation,
230 60°C 30 s joint annealing-extension and 60°C 30 s fluorescence measurement. Standard
231 dilutions prepared from DNA of each enrichment respectively using primers *amoA*19F and
232 *amoA*629R ranged between 10^2 and 10^8 copies µl $^{-1}$. The efficiency of qPCR assays was
233 between 86.06 and 93.04% with an R^2 of ≥ 0.996.
234
235 **Sanger and NGS sequencing of marker genes and genomes**
236 In order to confirm purity and identity of cultures, 16S rRNA genes were amplified by PCR with
237 the archaea specific primer A109f (Großkopf et al., 1998), the universal primer Univ1492R
238 (Lane, 1991), the crenarchaea specific primer pair 771F/957R (Ochsenreiter et al., 2003) and
239 the fungal ITS region-specific primer pair ITS1F and TW13 (Taylor and Bruns, 1999).
240 Amplification of the *amoA* genes was performed by PCR using the primers *amoA*19F (Tourna
241 et al., 2008) and *amoA*629R (Arce et al., 2018). PCR products were purified using the
242 Monarch® PCR & DNA Cleanup Kit from New England Biolabs before being sequenced.
243

244 **Genome sequencing, assembly and comparative genomics**

245 DNA of our enrichments was shotgun sequenced using the NovaSeq 6000 (paired-end,
246 150 bp) platform at Novogene. Reads were trimmed and Illumina adapters were removed
247 using Trimmomatic (SLIDINGWINDOW:5:20 LEADING:5 TRAILING:5 MINLEN:50
248 HEADCROP:6) (Bolger et al., 2014). To obtain the full genomic sequences of the enriched
249 archaeal communities from the selected cultures, Nanopore sequencing on MinION Mk1C
250 (Oxford Nanopore Technologies plc., UK) was performed. For library preparation, extracted
251 genomic DNA was repaired with the NEBNext Companion Module (New England Biolabs
252 GmbH, GER), and then prepared for sequencing on a chemistry version 14 flow cell (R10.4.1,
253 FLO-MIN114) following the Ligation sequencing gDNA – Native Barcoding Kit 24 V14 (SQK-
254 NBD114.24) and flow cell (FLO-MIN114) protocols.

255 Nanopore sequencing was performed according to the following configurations: run-time of
256 the MinION Mk1C device was set for 72 hours, with a pore scan frequency of 1.5 hours, a
257 minimum read length of 200 bp, high-accuracy base calling, and active channel selection,
258 reserved pores, read splitting, trimming barcodes and mid-read barcode filtering enabled. The
259 following software versions were used: MinKNOW v22.10.7, Bream v7.3.5, Configuration
260 v5.3.8, Guppy v6.3.9 and MinKNOW Core v5.3.1. Resulting sequencing data was analyzed
261 with the following specifications: First, simplex base calling was carried out on a GPU node at
262 the Life Science Compute Cluster (LiSC) University of Vienna (Austria), using guppy-gpu
263 v6.4.2 and the dna_r10.4.1_e8.2_260bps_sup.cfg model for superior base calling. Secondly,
264 duplex base calling was achieved at a GPU Node at the LiSC University of Vienna (Austria),
265 following the recommended tutorial on: https://github.com/nanoporetech/duplex-tools using
266 dorado v0.1.1 (https://github.com/nanoporetech/dorado) with the
267 dna_r10.4.1_e8.2_260bps_fast@v4.0.0 fast model, followed by finding duplex pairs with
268 duplextools v0.2.20-3.10 (https://github.com/nanoporetech/duplex-tools) and dorado
269 stereo/duplex base calling with the dna_r10.4.1_e8.2_260bps_sup@v4.0.0 superior model.

270 Merged simplex and duplex reads were then investigated by performing quality control using
271 NanoPlot nanocomp v1.20.0 (De Coster et al., 2018) followed by filtering with filtlong v0.2.1

272 (https://github.com/rrwick/Filtlong) (--min-length 200; --keep_percent 90, and --target_bases
273 20 million). Filtered reads were then assembled using flye v2.9.1 in --nano_hq and --meta
274 mode with a target genome size of 3 Mbpm (Kolmogorov et al., 2020). Reads were mapped
275 with minimap2 v2.24 (Li, 2021), and then polished with racon v1.5.0
276 (https://github.com/isovic/racon) using the following settings (-m -8 -x -6 -g -8 -w -500). Finally,
277 consensus contigs were obtained with medaka v1.7.2 according to the
278 r1041_e82_260bps_sup_g632 model (https://github.com/nanoporetech/medaka). Basic
279 genome statistics were calculated with genometools by calling gt seqstat (Gremme et al.,
280 2013), and classified the genomes using gtdbtk v2.1.1 with the --full_tree option enabled
281 (Chaumeil et al., 2020). Genome completeness and contamination were estimated with
282 checkm2 v1.0.1 including the --allmodels option (Chklovski et al., 2022). After genome
283 comparison using drep v3.4.2 (Olm et al., 2017), genomes were finally annotated with eggnog-
284 mapper v2.1.9 (Buchfink et al., 2015; Cantalapiedra et al., 2021; Eddy, 2011; Huerta-Cepas
285 et al., 2019; Hyatt et al., 2010; Steinegger and Söding, 2017) including prodigal for gene
286 identification. Marker genes were identified with Metaxa2 2.2 (Bengtsson-Palme et al., 2013)
287 and the remaining contaminants of enrichments were estimated with kraken2 2.1.2 and
288 bracken 2.8 according to the PlusPFP database (Lu and Salzberg, 2020; Wood et al., 2019)
289 (https://benlangmead.github.io/aws-indexes/k2).
290 Gene prediction and annotation of the MAGs assembled in this study was performed
291 automatically using the Microscope annotation platform from Genoscope (Vallenet et al.,
292 2020), followed by extensive manual curation. Annotations were supplemented with arCOG
293 assignments from the archaeal Clusters of Orthologous Genes database (2018 release)
294 (Makarova et al., 2015), Carbohydrate-active enzymes assignments (CAZymes) from
295 dbCAN2 (v7.0) (Zhang et al., 2018) and TCDB family assignments from the Transporter
296 Classification Database (Saier et al., 2016), using scripts from (Dombrowski et al., 2020).
297 Orthologous protein families from a dataset including *Ca*. N. franklandianus C13, *Ca.* N.
298 oleophilus MY3, *Ca.* N. hydrocola G61, *Ca.* N. agrestis SS, and *Ca.* N. arcticus Kfb and the

299 two newly sequenced *Ca.* Nitrosocosmicus isolates R2S and T1S were constructed using
300 Orthofinder (v.2.5.4) with standard settings (Emms and Kelly, 2019).
301
302 **Study-cohorts for molecular-based analyses**
303 Forty-seven healthy individuals (group A1: female=11, male=10, age=20-40 years; group A2:
304 f=15, m=11, age=60-85 years) were recruited for an in-depth analysis of their skin microbiome,
305 and a subgroup of high vs. low skin archaeal carriers was selected based on quantitative
306 (*amoA* gene and 16S rRNA gene qPCR universal and archaea specific primers; data types:
307 Cquant1, Cquant2, and Cquant3; Supplementary Fig. 2) and qualitative (16S rRNA gene
308 amplicons universal and archaea specific primers; data types: Cqual1, Cqual2, and Cqual4;
309 Supplementary Fig. 2) observations for longitudinal investigations (group B1 (from A1): f=2,
310 m=4; group B2 (from A2): f=5, m=1) over the period of almost two years (6 time points; data
311 type: L). The sampling sites for A1/A2 were hand, outer arm, crook, armpit, forehead, part,
312 décolleté and back (n=7), and for B1/B2: forehead, décolleté, arms and back (n=4).
313 Supplementary Table S3 gives an overview on the demographic characteristics of all recruited
314 subjects.
315 Each subject completed a questionnaire with different categories, e.g., height and weight, skin
316 type, and detailed questions about their respective lifestyle (e.g., eating habits, smoking,
317 alcohol consumption, skin care, medications, animal contact, and hobbies).
318
319 **Skin measurements and sampling**
320 The forehead and the part, as well as both hands, forearms, crooks and armpits were swabbed
321 with pre-moistened (0.9 % (v/v) NaCl) swabs (one swab for each body site; BD BBL ™ Culture
322 Swab ™ EZ; Becton Dickinson, USA). NaCl was baked at 260°C for 24 h before solving in
323 PCR-grade water to remove DNA traces. The remaining body sites, including décolleté and
324 back (approximately 300 cm^2), were sampled with a pre-moistened surface-sampling
325 cellulose-sponge kit (VWR, 300-0229P). For the longitudinal sampling (cohort B1/B2, tp2-6),
326 only the forehead was sampled with the swab. After skin sampling, samples were immediately

327 frozen at -80°C until further processing. All skin sampling events were accomplished in a lab
328 that never handled AOA, and controls from the environment, sampling procedure, and sample
329 extraction were processed in parallel.
330 Measurements of the skin physiology was performed using the Cutometer(R) MPA580
331 (Courage + Khazaka, Germany), using the Tewameter (to determine the barrier function by
332 measuring the water loss; 30s, 3 times), the pH-meter, the Sebumeter (to determine the
333 sebum-content, 30s), and the Corneometer (to determine skin moisture). Each skin site was
334 measured three times and the mean of the measurements is reported in Supplementary
335 Tables S4 and S5. Further, the surface temperature of each region was determined using an
336 infrared thermometer (Future Founder, China).
337 The interpretation of skin parameters was done based on the recommended specifications by
338 the manufacturer, which are provided in Supplementary Table S6.
339
340 **DNA extraction, controls, amplicon sequencing, and qPCR of skin samples**
341 The DNA was extracted from swabs and sponges using the Purelink ™ Microbiome DNA
342 Purification Kit (Rectal or Environmental Swab Samples; Thermo Fisher Scientific, USA). For
343 the extraction from sponges (liquid sample extract from décolleté and back) one ml of the
344 sample was concentrated by centrifugation (20817 x g, 4°C; 10 min). The largest proportion
345 of the supernatant was removed, and the remaining 70 µl was used for bead beating with 800
346 µl of the S1 lysis buffer. Material and process controls were included in each step to control
347 for the DNA contamination of the used reagents. The DNA was stored at -20°C until further
348 downstream analyses.
349 Various targets were assessed using amplicon-based analyses: i) the archaeal 16S rRNA
350 gene region (nested PCR approach as described in (Pausan et al., 2019) and (Probst et al.,
351 2013)), the ii) *amoA* targeted approach (described in (Arce et al., 2018; Leininger et al., 2006;
352 Tourna et al., 2011)), and the iii) “universal” approach, targeting the microbial 16S rRNA gene
353 region (Walters et al., 2011). All primer sequences and PCR protocols are provided in
354 Supplementary Table S7.

355 Library construction and next-generation sequencing (Illumina MiSeq®) was performed at the
356 Core Facility Molecular Biology at the Center for Medical Research (Medical University of
357 Graz, Austria). In a first step, the DNA concentrations of the generated amplicons were
358 normalized using a SequalPrepTM normalization plate (Invitrogen) and subsequently each
359 sample was indexed with a unique barcode sequence by 8 cycles of indexing PCR. These
360 indexed Samples were pooled and purified by gel cuts before the library was run on an Illumina
361 MiSeq® instrument and the MiSeq® Reagent Kit v3 with 602 cycles (2 x 301 cycles).
362
363 **Bioinformatics and data analysis**
364 Resulting demultiplexed fastq reads were processed with QIIME2 (Bolyen et al., 2018)
365 versions 2018.11 through 2023.2. After quality control, denoising of reads was achieved with
366 DADA2 (Callahan et al., 2016) and truncation of forward reads at a length of 230bp and 120bp
367 for reverse reads, was only used for the archaea-specific amplicon (519F-806R), while no
368 truncation was set for all other amplicon constructs (universal: 515F-926R; and *amoA*: 19F-
369 629R). Resulting feature tables and representative sequences were deposited on our Github
370 repository (https://github.com/CME-lab-research/SkinArchaeome). Potential contaminants were
371 identified with decontam v.1.12 (Davis et al., 2018) using the prevalence mode with a threshold
372 of 0.5 and removed from downstream analysis. Representative sequences were classified by
373 a pre-trained Naïve-Bayes classifier based on the curated and trimmed SILVA138 database
374 (Klindworth et al., 2013) using RESCRIPt (Robeson et al., 2021) and the feature-classifier
375 classify-sklearn plugin (Bokulich et al., 2018). For phylogenetic metrics like UniFrac (Lozupone
376 and Knight, 2005), a rooted phylogenetic tree was generated with FastTree2 (Price et al.,
377 2010) based on a masked MAFFT alignment. Data normalization was achieved by scaling
378 with ranked subsampling and the q2-srs QIIME2 plugin (Heidrich et al., 2021) at Cmin 50, 100
379 and 1000 followed by calculating core metrics for alpha and beta diversity. Feature differentials
380 were determined with the QIIME2 plugins aldex2 (Fernandes et al., 2013), ANCOM (Lin and
381 Peddada, 2020), ANCOM-BC (Lin and Peddada, 2020), and the R packages ANCOM2
382 (https://github.com/FrederickHuangLin/ANCOM-Code-Archive) and MaAsLin2 (Mallick et al.,

383 2021) including time as a fixed effect and different subjects as a random effect where
384 applicable, while feature loadings were determined with the QIIME2 plugin DEICODE (Martino
385 et al., 2019). Longitudinal analysis covering feature volatility over time as well as other
386 numerical metadata categories like age, BMI or skin physiology measurements including i.e.
387 pH, skin fat or skin wetness were realized with the q2-longitudinal plugin in QIIME2 (Bokulich
388 et al., 2018). The same plugin was used to calculate linear-mixed-effect models of Shannon
389 diversity and weighted UniFrac distances along principal coordinate axis 1. Amplicons of the
390 *amoA* marker gene were processed in a similar way without read truncations for DADA2 and
391 read classifications by a pre-trained Naïve-Bayes classifier based on the *amoA* reference
392 database (Alves et al., 2018; Wang et al., 2021). Connection of 16S rRNA to *amoA* gene
393 information was achieved by following the tutorial at https://github.com/alex-bagnoud/Linking-
394 16S-to-amoA-taxonomy/. Prediction of metadata categories were realized with the q2-sample-
395 classifier QIIME2 plugin (Bokulich et al., 2018).
396
397 Custom python code for regressing all metadata categories:
398 To identify potential associations between taxa and recorded numerical and categorical
399 metadata an ordinary least squares (OLS) regression fit method was used with python's
400 statsmodels smf formula (statsmodels.regression.linear_model.OLS - statsmodels 0.15.0
401 (+8)). Microbial counts of the different investigated cohorts were first clr transformed and
402 filtered for less than 25% missing values. These values were then used as the response
403 variable in dependence of each individual, their sex, age, BMI, body site, the overall microbial
404 diversity indicated by the Shannon index (H'), and where applicable the time of sampling. The
405 model was then evaluated for each genus and recorded metadata according to their q-values
406 (FDR-corrected p-values) and estimated regression coefficients (python code available at
407 GitHub: https://github.com/CME-lab-research/SkinArchaeome).
408
409 Network analysis:

410 Network analyses were conducted to identify mutually exclusive and co-occurring clusters of
411 archaea and bacteria in our merged (archaea-specific and universal) 16S rRNA gene amplicon
412 dataset. After SRS normalization to Cmin = 100 and TSS and log transformations the 40 most
413 abundant taxa were represented as nodes within the network where node size reflects taxa
414 abundance, and edges indicate only positive associations of Spearman correlations between
415 pairs of taxa. Then, we used PCoA to ordinate the nodes in a two-dimensional plot, such that
416 correlating nodes were close together and anti-correlating nodes were far apart. In addition,
417 correlations of the network were further supported by the Sparse Co-Occurrence Network
418 Investigation for Compositional data (SCNIC) package
419 (https://github.com/lozuponelab/SCNIC) using the sparCC metric with default settings for
420 filterings and the R value, and bootstrap adjusted p-values.
421
422 Phylogenomic tree reconstruction:
423 A genome database was created comprising the two AOA genomes presented in this study
424 together with 141 MAGs and completely sequenced genomes (133 AOA and 8 non-AOA
425 genomes) from IMG, DDBJ, or NCBI databases followed by protein prediction using Prodigal
426 v2.6.3 (Hyatt et al., 2010). The workflow proposed by Graham et al. (2018) (Graham et al.,
427 2018) based on the archaeal single-copy gene collection (Rinke et al., 2013) was followed to
428 identify phylogenetic markers (e-value 10^{-10}) to reconstruct the phylogenomic tree. A total of
429 36 ribosomal protein families encoded in at least 100 out of the 143 genomes present in our
430 genome database were selected. Each protein family was aligned independently using
431 MAFFT 7.520 (Katoh and Standley, 2013) (L-INS-i algorithm) followed by the trimming of the
432 alignments using BMGE (Criscuolo and Gribaldo, 2010) with default parameters. Trimmed
433 protein families were concatenated using a custom python script and the concatenated
434 alignment was used to reconstruct a maximum likelihood (ML) phylogenomic tree in IQ-TREE
435 v2.2.2.7 (Minh et al., 2020) under the LG+C20+F+G model with 1000 ultrafast bootstrap
436 replicates.
437

438 Phylogenetic analysis of 16S rRNA sequences:

439 The identification of 16S rRNA sequences in our AOA genome database (see above) was
440 performed using Barrnap v0.9 (https://github.com/tseemann/barrnap). The 16S rRNA
441 sequence encoded in the MAG GCA_025930575.1 (NS-Epsilon) was used as a query in a
442 BLASTN search against the NCBI database to improve the sequence representation of this
443 sub lineage with environmental sequences. Sequences were aligned with the SINA v1.7.2
444 aligner (Pruesse et al., 2012) using the SILVA database SSU Ref NR 99 release 138.1
445 (Klindworth et al., 2013) with default parameters followed by the alignment of the skin ASVs
446 using MAFFT 7.520 (Katoh and Standley, 2013) (--addfragments option, L-INS-i algorithm).
447 The alignment was trimmed manually using AliView (Larsson, 2014). The maximum likelihood
448 phylogenetic tree was reconstructed using IQ-TREE v2.2.2.7 (Minh et al., 2020) with the best-
449 fit model TIM2e+I+R3 chosen by ModelFinder ("-m MFP") (Kalyaanamoorthy et al., 2017)
450 according to BIC (Bayesian Information criterion), SH-like approximate likelihood ratio test ("-
451 alrt 1000") (Guindon et al., 2010) and 1,000 ultrafast bootstrap replicates ("-bb 1000").

452

453 qPCR specific methods

454 A SYBR green-based quantitative real-time PCR (qPCR) approach targeting the archaeal
455 *amoA* gene (19F-629R) and the 16S rRNA gene of archaea (A806F-A958R) and bacteria
456 (Bac_331F-Bac_797R) was used to determine the abundance of AOA, all archaea and all
457 bacteria on selected body sites. Primers, reaction mixtures and thermocycler programs are
458 listed in Supplementary Table S17. All qPCRs followed the MIQE Guidelines.

459 qPCRs were performed with the Bio-Rad SsoAdvanced™ Universal SYBR® Green Supermix.
460 Each reaction contained 1µl of DNA template and 9µl of mastermix. The mastermix for the
461 archaeal *amoA* approach consisted of 5µl SsoAdvanced™ Universal SYBR® Green Supermix
462 (Bio-Rad), 1.25µl of each primer (1.25µM) and 1.5µl of PCR grade water. The mastermix for
463 the archaeal and bacterial 16S rRNA gene approach consisted of 5µl SsoAdvanced™
464 Universal SYBR® Green Supermix (Bio-Rad), 0.3µl of each primer (10µM) and 3.4µl of PCR
465 grade water. Amplifications were carried out in a Bio-Rad CFX96 Touch™ Real-Time PCR

466 Detection System. The qPCR cycling conditions were as follows: initial denaturation at 95°C
467 for 1.5min, followed by 45 cycles of denaturation for 15sec at 95°C, annealing for 30sec at
468 60°C, elongation for 40sec at 72°C, a final denaturation for 15sec at 95°C, 5sec at 60°C and
469 a storage temperature of 8°C. A plasmid containing the *amoA* gene of *Nitrososphaera*
470 *viennensis* with a starting concentration of 104.1ng/µl (pscA_Ampkan_AmoA, clone 3) was
471 used as a quantification standard in a 1:10 dilution series from 10^{-2} to 10^{-10}. Product specificity
472 was confirmed by melting curve analysis. All qPCR experiments were performed in triplicates
473 and the results were averaged for further calculations. Data from a previous experiment on
474 the total archaeal community (based on qPCR of the 16S rRNA gene) was also included in
475 the analyses. To account for the different area sizes of the sampled body sites, copy numbers
476 were adjusted to 300 cm^2 (*amoA* gene copies per 300 cm^2; see Supplementary Table S8).
477 The qPCR files were analyzed using the CFX Manager™ Software, version 3.1 and processed
478 with the R software, version 3.6.1 and Microsoft Excel.
479
480

481 # Results

482 **Cultivation of AOA from human skin**

483

484 Different types of inocula were used to initiate enrichment cultures under oxic conditions in the
485 presence of 0.5 mM ammonia as sole energy source. Pooled samples were used after
486 swabbing the face, neck, upper body, back, arms, and legs of different individuals. After 2 to
487 9 months, amplification and sequencing of archaeal 16S rRNA and *amoA* gene fragments
488 identified the presence of single AOA strains in initial enrichments. The usage of pooled
489 samples of three different individuals resulted in three enrichment cultures: *Ca.*
490 Nitrosocosmicus "T1S", "X2B", and "Z3A". A fourth enrichment culture was obtained from cut
491 fingernail edges as initial inoculum ("R2S") (details of enrichment source are provided in
492 Supplementary Table S2).

493 The current study focuses on two of the enrichment cultures, “T1S” and “R2S”, isolated from
494 skin swabs and fingernail clippings respectively. These enrichments exhibited high enrichment
495 of 88-98% based on microscopy and molecular techniques (Supplementary Fig. 3) and
496 stoichiometric conversion of ammonia to nitrite every 3-4 weeks (Fig. 1 A-B) after repeated
497 transfers over the course of more than a year in medium supplemented with 0.6 mM
498 ammonium, 2 mM of either sodium carbonate (R2S) or sodium bicarbonate (T1S) and an
499 antibiotic mix. No bacterial contaminants were detected via amplification of the bacterial 16S
500 rRNA gene (Supplementary Fig. 4), or by light and scanning electron microscopy
501 (Supplementary Fig. 3). Based on the sequenced internal transcribed spacer (ITS) region the
502 remaining contaminant in both enrichments was a single fungal species with 99% sequence
503 identity to *Exophiala* sp. DAOM 216391, a genus of fungi frequently found in manmade
504 environments and known to be an opportunistic pathogen of humans (Untereiner and Naveau,
505 1999; Usuda et al., 2021).
506 Cell growth of the two strains R2S and T1S correlated with nitrite production as determined
507 by quantification of *amoA* genes using qPCR, as has previously been shown for other AOA
508 (Fig. 1, A-B) (Abby et al., 2018; Alves et al., 2019; Tourna et al., 2011). The shortest generation
509 times based on nitrite production were approximately five days at 28°C. After the oxidation of
510 ~500 µM ammonium enrichments R2S and T1S reached cell densities of $2.16*10^5$ (± $1.68*10^4$)
511 and $1.18*10^6$ (± $1.05*10^5$) cells ml^{-1}, respectively. This is similar to the cell densities of *Ca.*
512 Nitrosocosmicus franklandianus C13 ($3.8*10^6$ cells ml^{-1}) (Lehtovirta-Morley et al., 2016) and
513 *Ca.* Nitrosocosmicus oleophilus MY3 ($1.6*10^6$ cells ml^{-1}) (Jung et al., 2016) after oxidation of
514 ~500 µM ammonium.
515 For light microscopy, putative AOA were observed as cocci with diameters between 1-2 µm
516 which frequently formed aggregates and were partly enclosed in putative extracellular
517 polymeric substances (EPS) (Supplementary Fig. 3). These morphological features are
518 comparable with those of previously published members of the genus *Ca.* Nitrosocosmicus
519 (Alves et al., 2019; Jung et al., 2016; Lehtovirta-Morley et al., 2016; Liu et al., 2021) and were
520 confirmed by scanning electron microscopy (Fig. 1, C-F).

521

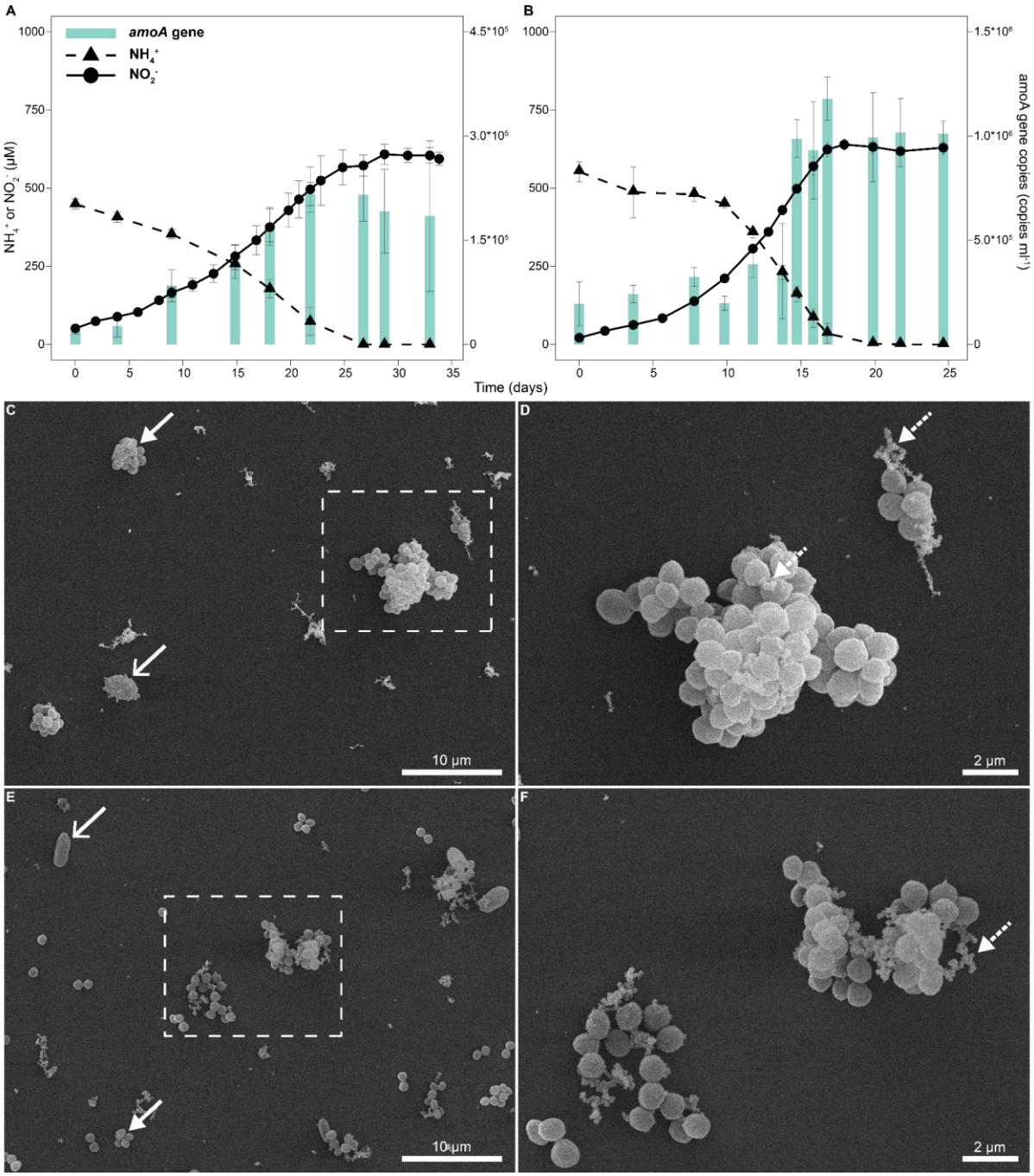

522

523

524 **Fig. 1.** Growth and morphology of skin enrichments R2S (A) and T1S (B) displaying near
525 stoichiometric conversion of ammonia (triangles, dashed line) to nitrite (circles, solid line)
526 paralleled by cell growth, estimated by qPCR of archaeal *amoA* gene copies (orange bars).
527 Ammonia and nitrite measurements are averages of biological triplicates. Gene copies of
528 *amoA* are averages of technical triplicates of each biological triplicate. Error bars depict the
529 standard deviation of the mean. Scanning electron micrographs of skin enrichments R2S (C,
530 D) and T1S (E, F) with white arrows indicating AOA cells based on the morphologies seen in
531 Supplementary Fig. 3 and already published members of the *Ca.* Nitrosocosmicus (Alves et
532 al., 2019; Jung et al., 2016; Lehtovirta-Morley et al., 2016; Liu et al., 2021). Dashed white

533 arrows indicate putative extracellular polymeric substances (D, F). Black arrows indicate the
534 remaining fungal contaminant.
535

536 **Taxonomic placement and genomic features of the AOA representatives from human**
537 **skin**

538 Sequencing and assembly of the genomes of the two skin enrichments resulted in one circular
539 contiguous sequence affiliated with AOA for each strain. The genome sizes, G+C content and
540 predicted protein-coding genes of the strains were well within the range of other
541 representatives of the genus *Ca.* Nitrosocosmicus (Table 1).
542 Like other representatives of this genus, both strains encoded three identical copies of the
543 16S and 23S rRNA gene operons. The average nucleotide identity (ANI) and average amino
544 acid identity (AAI) values between strains R2S and T1S (87.4% ANI, 86.2% AAI), and between
545 them and other *Ca.* Nitrosocosmicus genomes and proteomes were well below the threshold
546 of 95% ANI/AAI proposed for species delineation (Konstantinidis et al., 2017) (Supplementary
547 Tables S9 and S10). We therefore propose that they represent two distinct novel species,
548 preliminarily named *Ca.* Nitrosocosmicus epidermidis strain T1S (e.pi.der'mi.dis. Gr. fem. n.
549 epidermis, the outer skin; N.L. gen. n. epidermidis, of the epidermis) and *Ca.* Nitrosocosmicus
550 unguis R2S (un'gu.is. L. gen. n. unguis, of a fingernail).
551

552 **Table 1**: Genomic and growth features of *Ca.* Nitrosocosmicus epidermidis, *Ca.*
553 Nitrosocosmicus unguis compared to other cultivated representatives of the genus *Ca.*
554 Nitrosocosmicus
555

Organism#	Status	Growth temp (°C)	pH	Genome size (Mb)	No. of contigs	Completeness [%]	Contamination [%]	DNA GC %	protein coding genes	16S/23S/5S rRNA gene copies	reference
Nitrosocosmicus unguis R2S	Enriched	28	7	3.21	1	97.27	0.61	33.77	3597	3/3/1	this study
Nitrosocosmicus epidermidis T1S	Enriched	28	7	3.07	1	99.94	2.2	33.55	3401	3/3/1	this study
***N.* oleophilus MY3**	Pure	30	6.5-7	3.43	1	99.76	0.54	34.14	3722	3/3/1	Jung et al. 2016
***N.* franklandianus C13**	Pure	40	7	2.84	1	99.22	0.15	34.07	3025	2/2/1	Lehtovirta-Morley et al. 2016
***N.* arcticus Kfb**	Enriched	28	6	2.65*	23	98.67	0.19	34	2970	3/3/1	Alves et al. 2019
***N.* hydrocola G61**	Enriched	33	8	2.99	1	99.76	0.48	33.94	3162	2/2/1	Sauder et al. 2017
***N.* agrestis SS**	Enriched	37	6.5-7	3.22**	43	96.1	2.91	33.42	3524	2/2/1	Liu et al. 2021

556 # all organisms have Candidatus status
557

558 A maximum likelihood analysis based on 36 concatenated ribosomal protein marker genes
559 present in one copy in at least 100 of the 143 genomes of a dataset comprising representative
560 AOA and non-AOA of *Nitrososphaeria* confirmed the affiliation of the two novel strains with
561 the NS-zeta lineage as defined by Alves et al. 2018 (Alves et al., 2018). Specifically, the two
562 strains formed a highly supported cluster with *Ca.* N. arcticus (obtained from Arctic soil), *Ca.*
563 N. oleophilus (from coal-tar contaminated sediment), and other uncharacterized MAGs (Fig 2,
564 and Supplementary Table S9-S11).
565

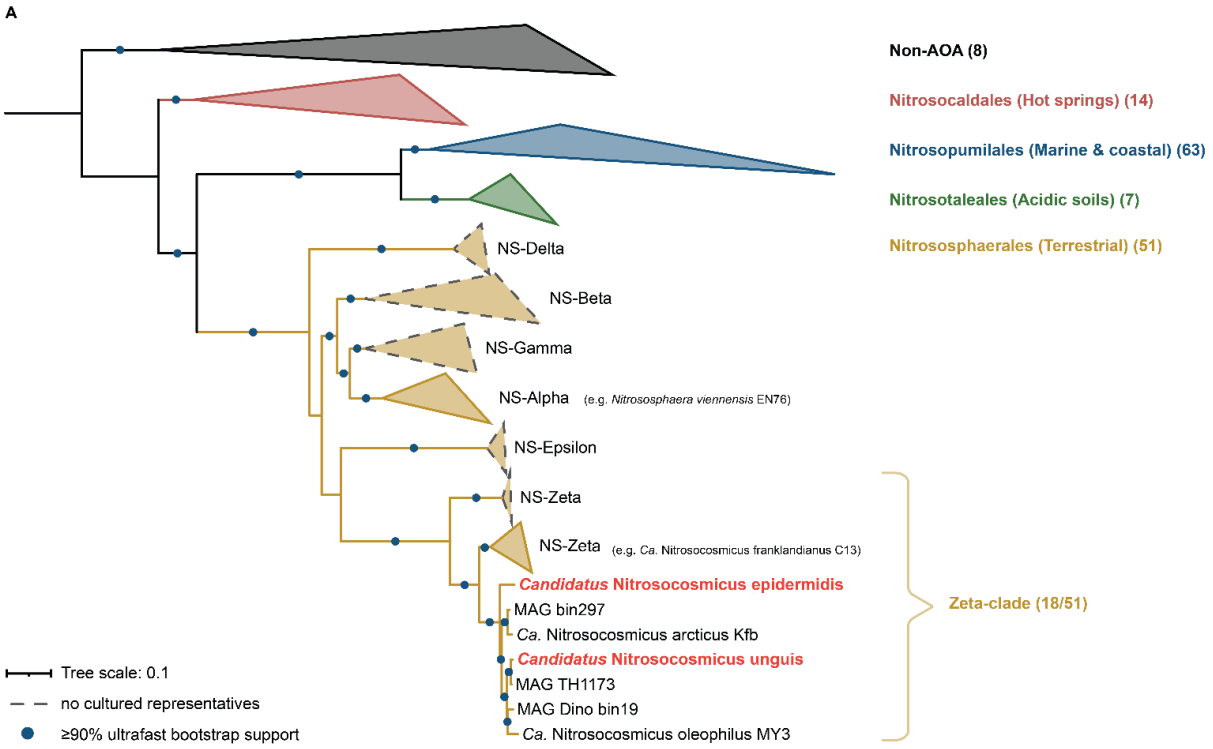

B

Domain desctiption	Domain ID	NS-ζ							NS-α		NT-α
		N.arc	N.frank	N.oleo	N.hydr	N.agr	N.ung	N.epid	N.vie	N.ever	N.deva
Sialidases											
Sialidase superfamily	IPR036278	2	7	13	9	9	4	5	7	11	4
Putative Lipases											
alpha/beta hydrolase fold	PF00561	5	8	14	7	9	13	12	5	6	1
alpha/beta hydrolase fold 1	PF12697	2	4	3	3	2	1	5	1	3	0
Alpha/beta hydrolase fold-3	PF07859	2	2	2	4	2	1	2	0	1	0
Patatin-like phospholipase domain	PF01734, arCOG09020	3	7	15	11	5	14	4	2	6	1
PLipase/COase/thioEstase	PF02230	1	1	1	1	1	1	2	0	1	0
Palmitoyl protein thioesterase	PF02089	1	1	1	0	1	3	2	0	0	0
Adhesion-related and surface recognition-related domains											
Tol-Pal_TolA	IPR014161	1	1	1	1	0	1	1	0	0	0
WD40/YVTN repeat-like-containing domain superfamily	IPR015943	12	14	23	20	19	15	13	6	9	9
NHL repeat, Six-bladed beta-propeller *	PF01436	5	5	5	5	6	6	2	0	0	4
Kelch-type beta propeller	PF01344	2	3	2	4	3	3	2	1	1	0
AdhesinB	IPR006129	2	2	2	2	2	2	2	2	1	1
Hemopexin-like repeats	PF00045	0	0	1	1	0	1	0	0	0	0
HYR domain	PF02494	1	1	1	1	1	1	1	4	2	3
Immunoglobulin-like fold	IPR013783	2	8	4	5	7	4	3	18	20	21
Coagulation factor 5/8 C-terminal domain	IPR000421	1	1	1	4	1	1	1	3	3	0
hyalin	PF02494	1	1	1	1	1	1	1	4	2	3
fibronectin	SSF49265, PS50853	0	0	0	0	0	1	0	1	0	12
Virulence-associated and interaction-associated domains											
Hemolysin-type calcium-binding conserved site	IPR018511	0	3	0	0	2	3	4	1	1	0
1.C.11 RTX Toxin Family; Serralysin-like metalloprotease	IPR011049, PF00353, arCOG11990	0	4	2	2	4	4	6	2	2	1
Cysteine-rich secretory protein-related	IPR001283	0	1	4	5	0	7	1	0	0	0
Ser-rich repeat protein, Dentin sialophosphoprotein-like/AT-2 Family**	no identifiable domain/OG0001706	1	1	1	1	1	1	1	0	0	0
Peptidases											
Calcineurin-like phosphoesterase domain, ApaH type	PF00149	4	3	4	3	4	4	5	2	2	4
Subtilisin-like serine protease	IPR015500	2	4	3	4	3	4	5	1	1	2
Peptidase M10, metallopeptidase, matrixin	PF00413	1	1	1	1	1	1	1	2	1	4
Peptidase S1C	PF13180	4	4	4	5	3	4	4	4	4	3
Peptidase C1A, papain C-terminal	PF00112	0	1	0	1	0	1	1	0	0	0
Peptidase S8/S53 domain, subtilisin-related	PF00082	2	5	4	4	3	4	5	1	2	2
Peptidase M48	PF01435	1	1	1	2	1	1	1	1	1	0
Peptidase M32, carboxypeptidase Taq	PF02074	1	1	1	1	1	1	1	0	1	0
Serine aminopeptidase, S33	PF12146	2	5	5	5	2	5	2	1	2	1
Peptidase M23	PF01551, arCOG11616	2	1	2	1	1	5	3	0	0	0
Beta-lactamase/transpeptidase-like	SSF56601	1	4	3	6	5	3	0	0	0	0
Peptidase M3A/M3B catalytic domain	PF01432	1	1	2	2	1	1	1	1	1	1
Peptidase_M50	PF02163	1	2	2	1	2	2	3	3	3	2
Peptidase M10, metallopeptidase	PF00413	1	1	1	1	1	1	1	2	1	4

* also found in serine/threonine protein kinases in diverse pathogenic bacteria

** Serine-rich repeat protein, Dentin sialophosphoprotein-like & 1.B.40 The Autotransporter-2 (AT-2) Family

Fig. 2. (A) Maximum-likelihood phylogenomic tree of AOA and non-AOA reconstructed based on the concatenated alignment of 36 ribosomal proteins comprising a total of 4,707 amino acid sites. Numbers in parentheses represent the number of complete genomes and MAGs in each lineage. NS = Nitrososphaerales. (B) Heatmap displaying the detection frequency of specific functional domains discussed in the text in all analyzed *Ca.* Nitrosocosmicus genomes.

572 Numbers refer to the number of occurrences of the respective domain in the genome, but do
573 not always correspond do distinct CDS (i.e. multiple domains on one CDS). Domain IDs refer
574 to Interpro, Pfam. TIGRfam, Superfamily Database entries.

575

576 To investigate the specific genomic repertoire of *Ca.* N. unguis and *Ca.* N. epidermidis, we
577 compiled a dataset consisting of the predicted proteomes of all available genomes from
578 cultivated strains of the genus *Ca.* Nitrosocosmicus: *Ca*. N. franklandianus C13, *Ca.* N.
579 oleophilus MY3, *Ca.* N. hydrocola G61, *Ca.* N. agrestis SS, and *Ca.* N. arcticus Kfb (we refrain
580 from the "Ca." prefix for better readability in the following). This protein dataset was clustered
581 into 3,301 orthologous protein families using Orthofinder (see Methods, Supplementary Data:
582 Orthologs, and Supplementary Table S12). From these orthologous protein families, 1,592
583 represented the core genome of the genus, comprising about 50% of the predicted CDS of
584 the genomes (Supplementary Table S13). The NS-Zeta subclade containing N. epidermidis,
585 N. arcticus, N. unguis and N. oleophilus shared 60 protein families N. unguis and N.
586 epidermidis shared only 20 protein families to the exclusion of all others, while both of them
587 shared more protein families with N. oleophilus (125 and 22 respectively) than any other *Ca.*
588 Nitrosocosmicus genome. The shell (=strain-specific) proteome of each skin isolate consisted
589 of 17 and 16 families for N. unguis and N. epidermidis respectively. The content of arCOG
590 functional categories did not differ among the *Ca.* Nitrosocosmicus genomes, indicating that
591 presence and survival on human skin did not require a particular expansion in a functional
592 category (Supplementary Fig. 5).

593

594 **A genomic island and expanded gene families implicate factors involved in host**
595 **interactions**

596 The *Ca.* N. *epidermidis* genome contains genomic islands flanked by integrases, encoding
597 proteins potentially involved in host interactions (Supplementary Data: Annotations). One such
598 island (Nepid_2202–2261) includes a putative autotransporter-1 (AT-1) family protein (TCDB:
599 (1.B.12), Nepid_2213) with extracellular domains of unknown function. These proteins

600 typically use a C-terminal β-barrel to export N-terminal virulence factors (van Ulsen et al.,
601 2018). In *Ca.* N. epidermidis, leucine-rich repeats on the N-terminal could facilitate protein–
602 protein recognition(Kobe, 2001). The island also encodes a putative α-arrestin-like protein
603 (Nepid_2245), containing arrestin N- and C-terminal domains (IPR011021 and IPR014752),
604 which in eukaryotes bind to and regulate 7TM and kinase receptors (e.g., GPCRs) (Alvarez,
605 2008). Though uncharacterized in prokaryotes, some pathogens exploit host β-arrestin
606 pathways to traverse epithelial barriers (Marullo and Coureuil, 2014). Additionally, the island
607 includes eight membrane-bound serine/threonine kinases and four serine-rich adhesins,
608 known in streptococci for mediating tissue and extracellular matrix binding (Chan et al., 2020).
609 In *Ca.* N. *unguis*, expanded gene families also suggest roles in host interaction (Fig. 2B,
610 Supplementary Data). Notably, it contains seven cysteine-rich secretory (CAP) family proteins
611 (vs. one in *Ca.* N. *epidermidis* and only a few in other *Ca.* Nitrosocosmicus genomes), a group
612 associated in eukaryotes with adhesion, signaling, and ion channel regulation, and potentially
613 linked to pathogenesis or antimicrobial defense (Gibbs et al., 2008; Yeats et al., 2003). *Ca.* N.
614 *unguis* is also enriched in beta-propeller fold proteins, which may mediate environmental
615 interactions through ligand binding, signaling, or enzymatic activity in the periplasmic space,
616 and are more abundant in *Ca.* Nitrosocosmicus than in other AOA lineages (Chen et al., 2011).
617

618 **Archaeal ammonia oxidizers form a rare, yet prevalent population on human skin**

619 A complementary, but independent approach was used to understand the abundance,
620 prevalence, distribution and stability of archaeal, and particularly *Ca.* Nitrosocosmicus
621 representatives on human skin. To achieve this, 47 healthy individuals were independently
622 recruited and eight defined body locations were sampled (cohorts A1 (age 20-40 years), A2
623 (60-80+ years), study overview: Supplementary Fig. 2 STORM chart, data types C). According
624 to their microbial profiles (high AOA, low AOA, see methods), 12 of these individuals were
625 then selected and longitudinally sampled on four body sites for an entire year (cohort B; study
626 overview: Supplementary Fig. 2, data types L). Samples were quantitatively (qPCR) analyzed
627 using taxonomic (16S rRNA) and functional (*amoA*) marker genes, targeted towards the

628 detection of archaea and archaeal ammonia oxidizers (AOA). As metagenomic sequencing
629 failed due to the low biomass and high background in human DNA, diversity assessments of
630 the skin archaeome were performed via amplicon sequencing to profile the bacterial, archaeal
631 and AOA-specific signatures. A total of 1,770 amplicons (PCR reactions (16S rRNA gene,
632 *amoA*) per sample including controls) were processed (details see Materials and Methods,
633 Supplementary Fig. 2, and Supplementary Table S14).
634 Throughout the study (cohorts A, B), archaeal signatures were found at least once in all study
635 participants, but were overall low, according to qPCR measurements (approx. 0.15±0.07%
636 relative abundance, average across all body sites; data types Cquant1, Cquant2, Cquant3).
637 AOA-specific qPCR signals accounted for $1.54*10^3$ gene copies per 300 cm^2 (Fig. 3A). The
638 highest amount of *amoA* gene copies were found in samples from the forehead (Fig. 3B);
639 there, AOA signatures were found in samples from every tested person at each time point
640 (prevalence: 100%; data types Lquant1, Lquant2, and Lquant3).
641 In amplicon sequencing, on average 6.88±4.67% of all samples contained archaea when the
642 universal PCR primer combination was applied (Supplementary Table S15, data types:
643 Cqual1 and Lqual1; Supplementary Fig. 2), whereas an average of 69.98±18.05% were
644 positive with the archaea-targeted combination of 16S rRNA gene primers (Supplementary
645 Table S8, data types: Cqual2 and Lqual2; Supplementary Fig. 2), emphasizing once more the
646 necessity to use archaea-targeted methodology for optimized detection. Also, with this
647 approach, all individuals were found to be positive for AOA signatures at least once throughout
648 the study period (on average 86±25%; $1.1*10^5$±$2.1*10^5$ reads of all samples).
649 Our independent approach with 16S rRNA gene sequencing detected most abundant AOA-
650 associated ASVs within the *Ca.* Nitrosocosmicus genus which matched the identified genus
651 from the cultivated enrichments (Fig. 3C). The most prevalent archaeal family within 326
652 samples (cohort A and B) was Nitrososphaeraceae (74% positive samples) with *Ca.*
653 Nitrosocosmicus being the most prominent genus in this family (24%) (Supplementary Table
654 S16; data types: Cqual2 and Lqual2; Supplementary Fig. 2). The joint classification of 16S
655 rRNA to the *amoA* marker gene (see Methods for details) resulted in a prevalence of 38% for

656 the NS-Zeta clade, across all samples (Supplementary Table S16; data types: Cqual2 and

657 Lqual2; Supplementary Fig. 2).

658

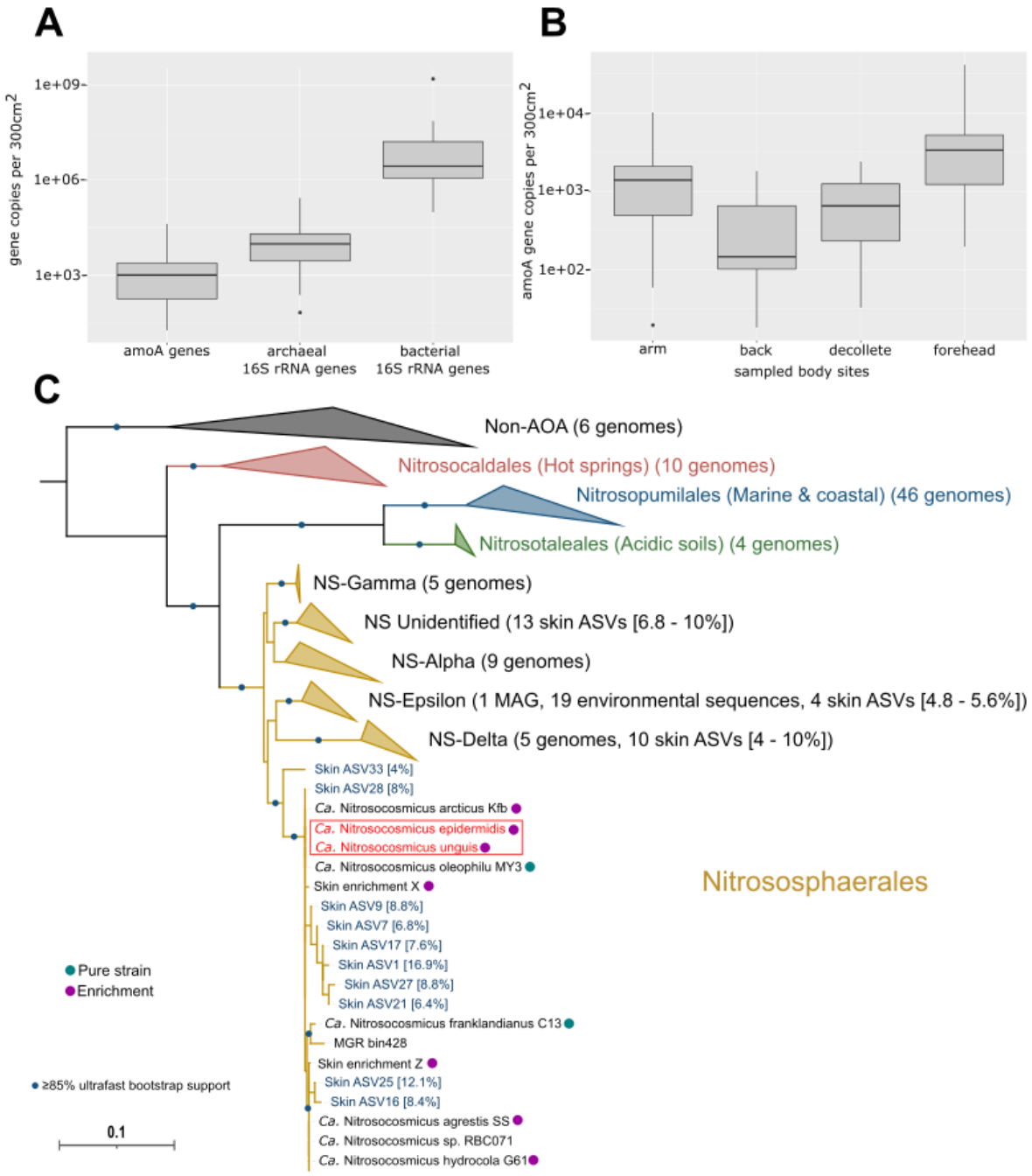

659

660 **Fig. 3.** (A and B) Quantitative analysis (qPCR) of AOA, archaeal and bacterial 16S rRNA gene
661 signatures on human skin (n=284; data types: Lquant1, Lquant2, and Lquant3; Supplementary
662 Fig. 2). The median of 16S rRNA gene copies across all sampling sites is shown; data are
663 corrected for different 16S rRNA gene copy numbers in archaea (median: 1) and bacteria (6);
664 https://rrndb.umms.med.umich.edu/). Gene copies per 300 cm^2 of AOA, Archaea and
665 Bacteria, shown on a logarithmic scaled Y-axis. (B) arm vs. back ($p = 5.9*10^{-4}$), arm vs.

666 decollete ($p = 7.2*10^{-4}$), arm vs. forehead ($p = 2.1*10^{-12}$), back vs. forehead ($p = 5.3*10^{-13}$),
667 decollete vs. forehead ($p = 6.1*10^{-13}$). *AmoA* gene copies per 300 cm^2, across sampling sites.
668 (C) Maximum-likelihood phylogenetic tree of 16S rRNA gene sequences of AOA and non-
669 AOA, including most prevalent and abundant ASVs of cohort A and B. Blue sequences
670 represent ASVs retrieved from amplicon sequencing of skin samples (cohorts A, B). Values in
671 brackets show the percentage of prevalence of the ASV in our samples.

672

673 ***Ca.* Nitrosocosmicus signatures show longitudinal coherence and unique**

674 **biogeographic patterns across body sites**

675 Across all eight body sites sampled (cohort A; data type: Cqual2; Supplementary Fig. 2),
676 Nitrososphaeraceae and *Ca.* Nitrosocosmicus signatures were mostly detected on forehead,
677 décolleté, back and arms, indicating a skin physiology-dependent pattern of ammonia-
678 oxidizing archaea in general (Fig. 4, 16S rRNA gene amplicons). High proportions of AOA
679 from the head region could be confirmed quantitatively (qPCR), as highest copy numbers of
680 the *amoA* gene (up to $4.11*10^4$ per 300 cm^2) were retrieved from the head samples (part and
681 forehead; Fig. 3B; data type: Lquant3; Supplementary Fig. 2).

682 *Ca.* Nitrosocosmicus signatures were stable longitudinally (1-year sampling period,
683 Supplementary Information; data type: Lqual2; Supplementary Fig. 2), and even individuals
684 that were not Archaea positive at the initial sampling time point became positive over the
685 course of the study period. In addition, participants who carried archaea at the initial time point
686 consistently showed archaeal signatures above the detection limit throughout all subsequent
687 time points (on average 78±10%; $1.4*10^5 \pm 9.4*10^4$ reads of all samples).

688 Seasons did not have a significant impact on the abundance of AOA (MaAsLin2, q-value =
689 0.95), indicating that contact with the outer environment, e.g. through contact to soil by
690 gardening work (MaAsLin2, q-value = 0.49; data type: Lqual2; see Supplementary Fig. 2
691 STORM chart for more details), did not influence the skin archaeome. We then tried to identify
692 AOAs on genus level that followed a longitudinal pattern by regression analysis. Signatures
693 assigned to *Ca.* Nitrosocosmicus (global mean = 0.17; global variance = 0.09; importance =
694 0.17) and other genera of the family *Nitrososphaeraceae* (global mean = 0.33; global variance
695 = 0.15; importance = 0.12) achieved high importance in linear regression analysis over time

696 supporting our assumption that AOA represent a coherent longitudinal trait on human skin
697 (Supplementary Table S17; data type: Lqual2; Supplementary Fig. 2). Further information on
698 bacterial ammonia oxidizers can be found in the Supplementary Information.

699

700

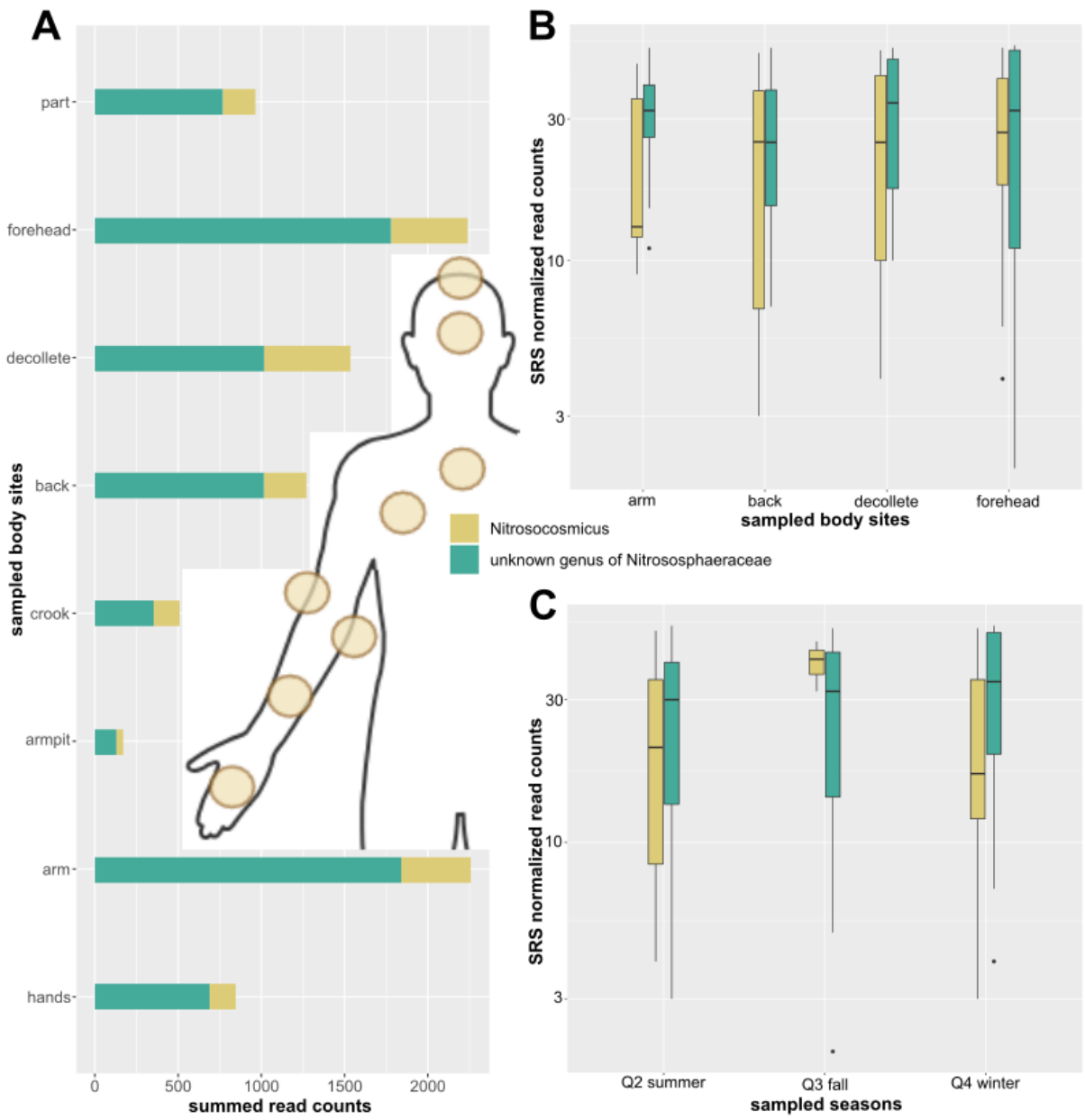

701

702 **Fig. 4.** (A) AOA prevalence across all samples from different body sites based on 16S rRNA
703 gene amplicon sequences, shown by summed read counts (n=326 samples; data types:
704 Cqual2; Supplementary Fig. 2). The reads obtained were assigned to *Ca.* Nitrosocosmicus

705 and other non-higher resolved genera belonging to the family Nitrososphaeraceae. Read
706 counts and percentage of all sampled body sites for *Ca.* Nitrosocosmicus (part: 197, 9%;
707 forehead: 461, 21%; décolleté: 519, 24%; back: 256, 12%; crook: 156, 7%; armpit: 41, 2%;
708 arm: 418, 19%; hands: 157, 7%). Read counts and percentage of all sampled body sites for
709 all AOA (part: 964, 10%; forehead: 2239, 23%; décolleté: 1535, 16%; back: 1271, 13%; crook:
710 509, 5%; armpit: 170, 2%; arm: 2258, 23%; hands: 846, 9%). (B) Boxplot showing the
711 abundance of AOA (normalized read counts) per body site. (C) Boxplot showing AOA
712 dynamics (normalized read counts) across the three covered seasons. Both B) and C) show
713 read counts on a log-scaled Y-axis and refer to the data of the longitudinal cohort (1-year, 6
714 time points, 3 seasons, 4 body sites, 283 samples; data type: Lqual2; Supplementary Fig. 2).

715

716 **AOA are an integral component of the healthy human skin microbiome**

717 Network analyses (data types: Lqual1 and Lqual2; Supplementary Fig. 2) were performed to
718 understand the integration of AOA into the skin microbiome. These showed a significant
719 positive correlation of *Ca.* Nitrosocosmicus with integral bacterial members of the human skin
720 microbiome (in particular *Lawsonella* and *Finegoldia* SCNIC sparCC p-adjust 0.26; see also
721 initial *in silico* metabolic modeling in Supplementary Fig. 6). In contrast to other microbiome
722 components, this interaction was relatively stable across all sampling time points (Fig. 5A, as
723 visualized by the dark color of the node, see legend). A specific integration of *Ca.*
724 Nitrosocosmicus into the skin microbiome network was underscored by the lack of positive
725 correlations of other archaeal signatures that are not common on human skin (e.g.,
726 *Methanobrevibacter*).

727

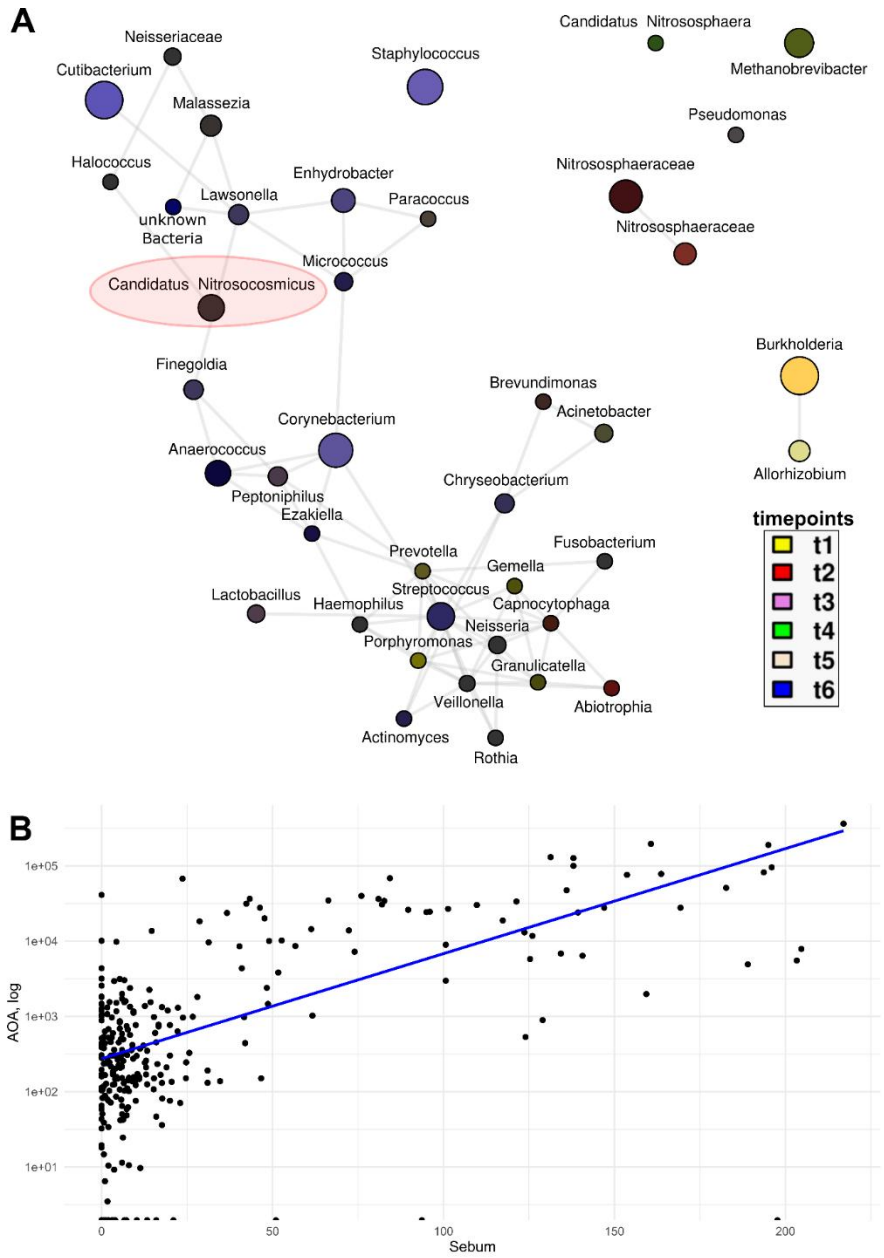

728

729

730 **Fig. 5.** (A) Microbial co-occurrence network (n = 283; data types: Lqual1 and Lqual2;
731 Supplementary Fig. 2) between the 40 most abundant archaeal and bacterial taxa (SRS
732 normalized Cmin = 100, TSS and log transformed). Significant positive associations from
733 Spearman correlations are highlighted by connecting edges. Taxa (nodes) were colored
734 according to color mixtures of each sampling event (t1 yellow, t2 red, t3 pink, t4 green, t5
735 beige, t6 blue), resulting in dark gray colors for longitudinally consistent taxa in the dataset.
736 The location of *Ca.* Nitrosocosmicus within the network is highlighted by a red ellipse. (B)
737 Spearman correlation plot of AOA signatures and sebum content of the skin.

738

739 Ordinary least squares (OLS) regression models were used to find associations between
740 archaeal taxa and acquired metadata (skin physiology, demographics of the cohort and their
741 lifestyle as well as health parameters; data type: Cqual2; Supplementary Fig. 2). Considering
742 the compositional nature of our amplicon datasets we used CLR (center log ratio) transformed
743 values and regressed them with all numerical and categorical metadata categories while
744 taking care of several potential confounders (which partly had significant impact on the
745 microbial communities) like a subject's sex, age, BMI, different sampled body sites and the
746 overall microbial diversity (Shannon diversity). According to this analysis, signatures of
747 Nitrososphaeraceae (n = 156) were significantly positively associated (q = 0.02) with qPCR-
748 retrieved quantity for AOA (Supplementary Table S18). This finding supports the congruence
749 of amplicon-based qualitative and qPCR-based quantitative molecular analyses.
750 The abundance of *amoA* genes as detected by qPCR (tp1, n=48) was not significantly
751 influenced by sex (female vs. male) and age group (group A1 (20-30 years) and A2 (>60
752 years)). However, the abundance of *amoA* signatures negatively correlated with lower pH
753 (rho= -0.081, p=0.174), and significantly negatively with increasing age (rho=-0.16, $p=7.7*10^{-}$
754 ^{3}), trans-epidermal water-loss ("Tewameter", rho=0.22, $p=4.8*10^{-4}$), and particularly sebum
755 concentration (rho=0.47, $p=1.0*10^{-16}$) according to Spearman rank correlations (data type:
756 Cquant3; Supplementary Fig. 2).
757
758 To assess the possibility whether AOA are involved in psoriatic disease, as hypothesized
759 earlier (Probst et al., 2013), 20 subjects were recruited and n=72 samples from lesioned and
760 healthy skin samples were taken (Cohort C, data type: P; Supplementary Fig. 2). However,
761 according to differential abundance analysis based on ANCOM-BC (p adjust = 0.07) and
762 MaAsLin2 (q-value = 0.54) samples from psoriatic skin did not reveal significantly higher or
763 lower AOA counts (data type: Pqual2; Supplementary Fig. 2).
764

765 ## Discussion

766

767 In this study, we demonstrate the consistent presence of AOA of the genus *Ca.*
768 *Nitrosocosmicus* on human skin, using two independent, but complementary, approaches:
769 cultivation and molecular profiling. Collectively, our results suggest that *Ca.* Nitrosocosmicus
770 representatives are an integral component of the skin microbiome. This conclusion is
771 supported by:
772 (i) the repeated enrichment of *Ca.* Nitrosocosmicus strains from independent human skin
773 samples
774 (ii) unique genomic features indicative of habitat-specific adaptation
775 (iii) their high prevalence and distinct biogeographic patterns in molecular analyses, and
776 (iv) specific co-occurrence with established skin-associated bacterial taxa

777

778 These findings not only highlight the ecological relevance of *Ca. Nitrosocosmicus* on human
779 skin but also raise important questions regarding their functional role. Both highly enriched
780 AOA cultures exhibited a stoichiometric conversion of ammonia to nitrite that is typical of other
781 isolated AOA species, and their genomes encode urease, enabling urea utilization. Given that
782 ammonia and urea are the primary nitrogenous species excreted on human skin through
783 sweat (Chen et al., 2020), these substrates likely represent a stable energy source for these
784 organisms.
785 Although the archaeal ammonia oxidation pathway has yet to be resolved, the intermediate
786 nitric oxide (NO) has been observed to play a critical role for these organisms (Jessica A
787 Kozlowski et al., 2016). Since NO is one of the most important signaling molecules in
788 mammalian physiology, and is involved in a range of physiological as well as pathological
789 processes on the human skin (reviewed in (Cals-Grierson and Ormerod, 2004; Suschek et al.,
790 2010)), AOA could contribute to the maintenance of NOx homeostasis on the human skin and
791 thereby play a role in skin health or physiology. It is also worth noting that nitrite, the final

792 product of nitrification, also serves as a signaling molecule in a NO-independent manner
793 (Bryan et al., 2005; Gladwin et al., 2006).
794 Both enriched strains were placed phylogenetically within the genus *Ca.* Nitrosocosmicus, a
795 genus that was also consistently detected in cohorts A and B of an independent cross-
796 sectional as well as longitudinal study. Although the relative abundance appears low in these
797 human samples, it is not outside the range observed for AOA in other environments (Alves et
798 al., 2019; Leininger et al., 2006).
799 To date, *Ca.* Nitrosocosmicus species have predominantly been isolated from soil
800 environments, and are known for their aggregate structures, propensity to grow in biofilms,
801 and superior adhesion capacities (Dreer et al., 2024; Jung et al., 2016; Liu et al., 2021). These
802 traits are supported by the specific encoding or expansion of adhesion proteins, acetamido
803 sugar biosynthesis and export proteins, as well as protein families whose products can directly
804 interact with and modulate other organisms, such as peptidases, phospholipases and
805 triacylglycerol esterases/lipases ((Jung et al., 2016; Liu et al., 2021) and this study), with
806 known roles in tissue invasion and colonization, virulence and mediation of the host immune
807 response (Garcia et al., 2018).
808 All of these features support the interaction of this genus with a variety of species in their
809 respective environments and is further supported by recent evidence of *Ca.* Nitrosocosmicus
810 associations and interactions with the plant rhizosphere (Lee et al., 2024) . The strains *Ca.* N.
811 epidermidis and *Ca.* N. unguis share these genomics features while also displaying unique
812 attributes suggestive of skin-specific functions.
813 Host interaction capabilities and attachment strategies are well established among skin-
814 associated microorganisms (Brandwein et al., 2016), and our data indicate that *Ca. N.*
815 *epidermidis* exhibits similar potential. Its genome harbors a genomic island that is enriched in
816 proteins that facilitate surface adhesion and interactions with various tissue types and proteins
817 that could putatively interact with eukaryotic proteins including an autotransporter (Mondal et
818 al., 2022) and arrestin-like protein (Alvarez, 2008; Marullo and Coureuil, 2014). Similarly, *Ca.*
819 N. unguis has an unusually high amount of cysteine-rich secretory protein (CAP) family

820 proteins and beta propeller fold containing proteins that are both known for mediating
821 interactions with the surrounding environment including signaling and regulation of host
822 proteins (Chen et al., 2011; Gibbs et al., 2008; Yeats et al., 2003). The distinct repertoire of
823 each strain may reflect micro-habitat preferences on the heterogeneous skin landscape.
824 Currently, it remains difficult to unequivocally identify proteins that are specific to the skin
825 environment, but this is not a *Ca.* Nitrosocosmicus-specific difficulty; many skin-associated
826 microorganisms display ecological flexibility occupying both, mammalian host-associated and
827 environmental niches. Such dual lifestyles are well documented across microbial taxa.
828 This holds true for archaea in the case of the order Methanomassiliicoccales, which are able
829 to thrive in both the gastrointestinal tract of mammals and diverse natural habitats (Cozannet
830 et al., 2020; De La Cuesta-Zuluaga et al., 2021), as well as for many opportunistic pathogens
831 of bacteria including *Vibrio sp.* (aquatic environments(Soto and Nishiguchi, 2021)),
832 *Stenotrophomonas maltophilia* (soil, plant environments (Brooke, 2012)), or *Bukholderia*
833 *pseudomallei* (Ghazali et al., 2023). The constant interaction between host and environment
834 can further confound the identification of host-related proteins without further in-depth analysis
835 of individual strains.
836 Regardless, the consistent presence of AOA on human skin within the longitudinal
837 study supports the proposal of *Ca.* Nitrosocosmicus sp. being an emerging commensal skin
838 microorganism. Their presence was found to be independent of age, sex, or time of year
839 suggesting that they are a stable and integral component of the microbial epidermal skin
840 microbiome. The detected presence additionally showed correlations with skin parameters,
841 in particular a positive correlation with sebum content. Sebum is an oily substance that
842 contains many lipids with hydrophobic properties and this correlation suggests that this AOA
843 lineage can thrive in this type of environment. This fits not only with the several lipid interaction
844 genes found within *Nitrososcosmicus,* but also with the placement of *Ca.* N. epidermidis, *Ca.*
845 N. unguis, and several skin AOA ASVs next to the AOA species *Ca.* N. *oleophilus* which was
846 isolated from coal-tar contaminated soil and exhibited a strong affinity for hydrophobic
847 surfaces (Jung et al., 2016). The positive correlations with both the genera *Lawsonella* and

848 *Finegoldia* are also revealing as both have been associated with high sebum areas such as
849 the forehead ((Kim et al., 2021; Li et al., 2024).These co-occurrence patterns may reflect
850 ecological interdependencies or shared niche preferences.

851 The metabolic activity of AOA, particularly their role in nitrogen cycling, may be crucial in
852 shaping the skin microbiome. Given the scarcity of AOB on human skin, AOA likely fulfill this
853 ecological function. Additionally, the capacity to produce crucial vitamins, such as B12 (Bayer
854 et al., 2019), via an autotrophic metabolism may also play an important role in the community
855 structure of the skin microbiome as it does in other environments.
856 Their interactions with integral bacterial members of the human microbiome may also have a
857 positive impact on the host that is so far unknown, as no association with psoriasis was found.
858 Nevertheless, many aspects of skin health remain unexplored in the context of archaeal
859 involvement. Based on our findings, we can conclude, that *Ca.* Nitrosocosmicus is an integral
860 and stable component of the microbial epidermal skin microbiome that is associated with
861 relevant bacteria potentially via the exchange of ammonia and is characteristic of healthy skin
862 with higher sebum content, less moisture and lower pH.
863

864 Conclusions

865 In conclusion, this study marks the first AOA enrichments obtained from human skin
866 and confirms the presence of the obtained genera, *Ca.* Nitrosocosmicus, on a wide range of
867 individuals of varying sex and age. Initial genomic and physiological observations suggest that
868 these AOA are adapted for growth on hydrophobic tissue surfaces as both enriched strains
869 contain unique genes and protein families compared to other *Ca.* Nitrosocosmicus species
870 involved in either adhesion or extracellular protein interaction. Further studies of skin archaea
871 will be needed to reveal their evolutionary paths towards commensalism and to elucidate their
872 roles in the skin microbiome and human health. The archaeal cultures obtained in this study
873 are crucial prerequisites for advancing our knowledge in this area.
874

875

876 **List of abbreviations**

877 Ammonia-oxidizing archaea (AOA)

878 ammonia monooxygenase subunit A gene (amoA)

879 nitric oxide (NO)

880 Deoxyribonucleic Acid (DNA)

881 Ribonucleic Acid (RNA)

882 Polymerase chain reaction (PCR)

883 Quantitative polymerase chain reaction (qPCR)

884 freshwater medium (FWM)

885 3-(N-morpholino) propanesulfonic acid (MOPS)

886 Hydrogen chloride (HCl)

887 Phosphate buffered saline (PBS)

888 High molecular weight (HMW)

889 mixed cellulose ester (MCE)

890 Oxford Nanopore Technologies (ONT)

891 Life Science Compute Cluster (LiSC)

892 archaeal Clusters of Orthologous Genes (arCOG)

893 Carbohydrate-active enzymes assignments (CAZymes)

894 Quantitative Insights Into Microbial Ecology (QIIME)

895 Divisive Amplicon Denoising Algorithm (DADA)

896 Multiple Alignment using Fast Fourier Transform (MAFFT)

897 Analysis of Compositions of Microbiomes with Bias Correction (ANCOM-BC)

898 Microbiome Multivariable Associations with Linear Models (MaAsLin)

899 ANOVA-Like Differential Expression tool (Aldex)

900 Differential Eigenvalue Interpretation for Compositional Omics Data Exploration (DEICODE)

901 Reference Sequence Curation Pipeline Tool (RESCRIPt)

902 ordinary least squares (OLS)

903 center log ratio (CLR)

904 false discovery rate (FDR)

905 metagenome assembled genome (MAG)

906 Body Mass Index (BMI)

907 Principal Coordinates Analysis (PCoA)

908 Principal Component Analysis (PCA)

909 Sparse Cooccurrence Network Investigation for Compositional data (SCNIC)

910 maximum likelihood (ML)

911 SILVA Incremental Aligner (SINA)

912 Small Subunit (SSU)

913 Basic Local Alignment Search Tool for Nucleotides (BLASTN)

914 Average Nucleotide Identity (ANI)

915 Amino Acid Identity (AAI)

916 Nitrososphaerales (NS)

917 Amplicon Sequence Variant (ASV)

918

919 Declarations

920

921 Ethics approval and consent to participate

922 Subjects for microbiome analyses were recruited as part of the project "Detection of Archaea
923 on Healthy and Diseased Skin" with the ethical vote EK: 27-289 ex 14/15 (Medical University
924 of Graz) and all ethical requirements were followed and fulfilled including an informed
925 consent to participate in the presented study. The following exclusion criteria were taken into
926 account: Antibiotics therapy within the last three months, pregnancy, ongoing breast-feeding
927 and non-compliance. The participants were asked to not shower or apply skin cream the day
928 before sampling.

929

930 **Consent for publication**

931 All authors approved the manuscript and give their consent for publication.

932

933 **Availability of data and material**

934 All raw sequencing data were submitted to NCBI's Sequence Read Archive (SRA)
935 https://www.ncbi.nlm.nih.gov/sra and are accessible under the following projects:
936 PRJNA1105887 (archaea specific 16S rRNA gene amplicons of cohort A; data type: Cqual2),
937 PRJNA1107153 (universal 16S rRNA gene amplicons of cohort A; data type: Cqual1),
938 PRJNA1107462 (AOA specific *amoA* gene amplicons of cohort A; data type: Cqual4),
939 PRJNA1107502 (archaea specific 16S rRNA gene amplicons of cohort B; data type: Lqual2),
940 PRJNA1107512 (universal 16S rRNA gene amplicons of cohort B; data type: Lqual1),
941 PRJNA1105887 (archaea specific 16S rRNA gene amplicons of cohort C; data type: Pqual2),
942 PRJNA1108073 (universal 16S rRNA gene amplicons of cohort C; data type: Pqual1),
943 PRJNA1108908 (pooled shotgun metagenomics data of cohort A), PRJNA1108960 (Illumina
944 sequencing data of enrichments), PRJNA1109334 (Nanopore sequencing data of
945 enrichments). Assemblies are publicly available under NCBI BioProjects PRJNA1103140 (*Ca.*
946 Nitrosocosmicus epidermidis T1S) and PRJNA1103141 (*Ca.* Nitrosocosmicus unguis).
947 Annotated assemblies are also available at the MicroScope Microbial Genome Annotation and
948 Analysis Platform, developed by the Laboratory of Bioinformatics Analyses for Genomics and
949 Metabolism, Genoscope, Evry, France.

950

951 **Code availability**

952 The present study did not generate new code, and mentioned tools used for the data analysis
953 were applied with default parameters unless specified otherwise in Methods and our Github
954 repo. https://github.com/CME-lab-research/SkinArchaeome

955

956 **Competing interests**

957 The authors declare that they have no competing interests.

958

959 **Funding**

960 This research was funded in whole or in part by the Austrian Science Fund (FWF)
961 [10.55776/P30796, given to CME and CS; supported by grants: 10.55776/P32697(CME),
962 10.55776/CoE7 (CME), 10.55776/F8300 (CME) and 10.55776/Z437 (CS)]. Also funded by
963 ERC-2023-PoC:101138959. For open access purposes, the author has applied a CC BY
964 public copyright license to any author-accepted manuscript version arising from this
965 submission.

966

967 **Authors' contributions**

968 AM supervised and performed microbiome sampling and analysis. MD supervised and
969 performed cultivation and microscopy. MM and LH supervised and supported cultivation
970 work. UP performed cultivation. SD, AL, TG, DB performed sampling, sequencing, and data
971 analysis of qPCR and amplicon data. RP performed phylogenetic analyses and genome
972 assembly. TG and PW recruited patients and performed sampling. MK performed genome
973 annotations and contributed to study concept. CME and CS developed the study concept,
974 wrote initial proposal, and wrote, together with MK and AM the manuscript. All authors
975 contributed to the finalization of the manuscript.

976

977 **Acknowledgements**

978 We acknowledge the technical support by Ignaz Herzeg, Lisa Wink, Polona Mertelj, Sarah
979 Harrer and all collaborators at the Department of Dermatology and Venereology, Medical
980 University of Graz (Andrea Alejandra Catalan Griffiths, Patra Vijaykumar, Isabella Perchthaler,
981 Alexandra Gruber-Wackernagel, Wolfgang Weger, and univ. Prof. Dr. Wolfgang Salmhofer).
982 We thank Daniela Gruber from the Core Facility Cell Imaging & Ultrastructure Research
983 (LeWi).

We greatly value the computational resources of the MedBioNode provided by the Medical University of Graz and the Life Science Compute Cluster (LiSC) operated by the Computational Systems Biology group at the University of Vienna as well as the Medical University of Graz ZMF Galaxy Team: Core Facility Computational Bioanalytics, Medical University of Graz, funded by the Austrian Federal Ministry of Education, Science and Research, Hochschulraum-Strukturmittel 2016 grant as part of BioTechMed Graz.

SD was supported by the local PhD program MolMed.

References

Abby, S.S., Melcher, M., Kerou, M., Krupovic, M., Stieglmeier, M., Rossel, C., Pfeifer, K., Schleper, C., 2018. Candidatus Nitrosocaldus cavascurensis, an ammonia oxidizing, extremely thermophilic archaeon with a highly mobile genome. Front Microbiol 9, 346006. https://doi.org/10.3389/FMICB.2018.00028/BIBTEX

Alvarez, C.E., 2008. On the origins of arrestin and rhodopsin. BMC Evol Biol 8, 222. https://doi.org/10.1186/1471-2148-8-222

Alves, R.J.E., Kerou, M., Zappe, A., Bittner, R., Abby, S.S., Schmidt, H.A., Pfeifer, K., Schleper, C., 2019. Ammonia oxidation by the arctic terrestrial thaumarchaeote candidatus nitrosocosmicus arcticus is stimulated by increasing temperatures. Front Microbiol 10, 1571. https://doi.org/10.3389/FMICB.2019.01571/FULL

Alves, R.J.E., Minh, B.Q., Urich, T., Haeseler, A., Schleper, C., 2018. Unifying the global phylogeny and environmental distribution of ammonia-oxidising archaea based on amoA genes. Nat Commun 9, 1517.

Arce, M.I., von Schiller, D., Bengtsson, M.M., Hinze, C., Jung, H., Alves, R.J.E., Urich, T., Singer, G., 2018. Drying and Rainfall Shape the Structure and Functioning of Nitrifying Microbial Communities in Riverbed Sediments. Front Microbiol 9. https://doi.org/10.3389/fmicb.2018.02794

Bang, C., Schmitz, R.A., 2015. Archaea associated with human surfaces: not to be underestimated. FEMS Microbiol Rev 39, 631–648. https://doi.org/10.1093/femsre/fuv010

Bayer, B., Hansman, R.L., Bittner, M.J., Noriega-Ortega, B.E., Niggemann, J., Dittmar, T., Herndl, G.J., 2019. Ammonia-oxidizing archaea release a suite of organic compounds potentially fueling prokaryotic heterotrophy in the ocean. Environ Microbiol 21, 4062–4075. https://doi.org/10.1111/1462-2920.14755

Bengtsson-Palme, J., Ryberg, M., Hartmann, M., Branco, S., Wang, Z., Godhe, A., 2013. Improved software detection and extraction of ITS1 and ITS2 from ribosomal ITS sequences of fungi and other eukaryotes for analysis of environmental sequencing data. Meth Ecol Evol 4.

1022 Berg, G., Rybakova, D., Fischer, D., Cernava, T., Vergès, M.-C.C., Charles, T., Chen, X.,
1023 Cocolin, L., Eversole, K., Corral, G.H., 2020. Microbiome definition re-visited: old
1024 concepts and new challenges. Microbiome 8, 1–22.
1025 Bokulich, N., Dillon, M., Bolyen, E., Kaehler, B., Huttley, G., Caporaso, J., 2018. q2-sample-
1026 classifier: machine-learning tools for microbiome classification and regression. J Open
1027 Source Softw 3, 934. https://doi.org/10.21105/joss.00934
1028 Bolger, A.M., Lohse, M., Usadel, B., 2014. Trimmomatic: a flexible trimmer for Illumina
1029 sequence data. Bioinformatics 30, 2114–2120.
1030 https://doi.org/10.1093/bioinformatics/btu170
1031 Bolyen, E., Rideout, J.R., Dillon, M.R., Bokulich, N.A., Abnet, C., Ghalith, G.A. Al, Alexander,
1032 H., Alm, E.J., Arumugam, M., Bai, Y., Bisanz, J.E., Bittinger, K., Brejnrod, A., Colin, J.,
1033 Brown, C.T., Callahan, B.J., Mauricio, A., Rodríguez, C., Chase, J., Cope, E., Silva, R.
1034 Da, Dorrestein, P.C., Douglas, G.M., Duvallet, C., Edwardson, C.F., Ernst, M.,
1035 Fouquier, J., Gauglitz, J.M., Gibson, D.L., Gonzalez, A., Huttley, G.A., Janssen, S.,
1036 Jarmusch, A.K., Kaehler, B.D., Kang, K. Bin, Keefe, C.R., Keim, P., Kelley, S.T., Ley,
1037 R., Loftfield, E., Marotz, C., Martin, B., Mcdonald, D., Mciver, L.J., Alexey, V., Metcalf,
1038 J.L., Morgan, S.C., Morton, J.T., Naimey, A.T., 2018. QIIME 2 : Reproducible ,
1039 interactive , scalable , and extensible microbiome data science.
1040 https://doi.org/10.7287/peerj.preprints.27295
1041 Borrel, G., Brugère, J.F., Gribaldo, S., Schmitz, R.A., Moissl-Eichinger, C., 2020. The host-
1042 associated archaeome. Nat Rev Microbiol. https://doi.org/10.1038/s41579-020-0407-y
1043 Brandwein, M., Steinberg, D., Meshner, S., 2016. Microbial biofilms and the human skin
1044 microbiome. npj Biofilms and Microbiomes 2016 2:1 2, 1–6.
1045 https://doi.org/10.1038/s41522-016-0004-z
1046 Brooke, J.S., 2012. Stenotrophomonas maltophilia: an Emerging Global Opportunistic
1047 Pathogen. Clin Microbiol Rev 25, 2–41. https://doi.org/10.1128/CMR.00019-11
1048 Bryan, N.S., Fernandez, B.O., Bauer, S.M., Garcia-Saura, M.F., Milsom, A.B., Rassaf, T.,
1049 Maloney, R.E., Bharti, A., Rodriguez, J., Feelisch, M., 2005. Nitrite is a signaling
1050 molecule and regulator of gene expression in mammalian tissues. Nat Chem Biol 1,
1051 290–297. https://doi.org/10.1038/nchembio734
1052 Buchfink, B., Xie, C., Huson, D.H., 2015. Fast and sensitive protein alignment using
1053 DIAMOND. Nat Methods 12, 59. https://doi.org/10.1038/nmeth.3176
1054 Byrd, A.L., Belkaid, Y., Segre, J.A., 2018. The human skin microbiome. Nat Rev Microbiol
1055 16, 143–155. https://doi.org/10.1038/nrmicro.2017.157
1056 Callahan, B.J., McMurdie, P.J., Rosen, M.J., Han, A.W., Johnson, A.J.A., Holmes, S.P.,
1057 2016. DADA2: High-resolution sample inference from Illumina amplicon data. Nat
1058 Methods 13, 581–583. https://doi.org/doi:10.1038/nmeth.3869
1059 Cals-Grierson, M.-M., Ormerod, A.D., 2004. Nitric oxide function in the skin. Nitric Oxide 10,
1060 179–193. https://doi.org/10.1016/j.niox.2004.04.005
1061 Cantalapiedra, C.P., Hernández-Plaza, A., Letunic, I., Bork, P., Huerta-Cepas, J., 2021.
1062 eggNOG-mapper v2: Functional Annotation, Orthology Assignments, and Domain
1063 Prediction at the Metagenomic Scale. Mol Biol Evol 38, 5825–5829.
1064 https://doi.org/10.1093/molbev/msab293
1065 Chan, J.M., Gori, A., Nobbs, A.H., Heyderman, R.S., 2020. Streptococcal Serine-Rich
1066 Repeat Proteins in Colonization and Disease. Front Microbiol 11.
1067 https://doi.org/10.3389/fmicb.2020.593356

1068 Chaumeil, P.A., Mussig, A.J., Hugenholtz, P., Parks, D.H., 2020. GTDB-Tk: A toolkit to
1069 classify genomes with the genome taxonomy database. Bioinformatics 36, 1925–1927.
1070 https://doi.org/10.1093/bioinformatics/btz848
1071 Chen, C.K.-M., Chan, N.-L., Wang, A.H.-J., 2011. The many blades of the β-propeller
1072 proteins: conserved but versatile. Trends Biochem Sci 36, 553–561.
1073 https://doi.org/10.1016/j.tibs.2011.07.004
1074 Chen, Y.-L., Kuan, W.-H., Liu, C.-L., 2020. Comparative Study of the Composition of Sweat
1075 from Eccrine and Apocrine Sweat Glands during Exercise and in Heat. Int J Environ
1076 Res Public Health 17, 3377. https://doi.org/10.3390/ijerph17103377
1077 Chibani, C.M., Mahnert, A., Borrel, G., Almeida, A., Werner, A., Brugère, J.-F., Gribaldo, S.,
1078 Finn, R.D., Schmitz, R.A., Moissl-Eichinger, C., 2022. A catalogue of 1,167 genomes
1079 from the human gut archaeome. Nat Microbiol 7, 48–61.
1080 https://doi.org/10.1038/s41564-021-01020-9
1081 Chklovski, A., Parks, D.H., Woodcroft, B.J., Tyson, G.W., 2022. CheckM2: a rapid, scalable
1082 and accurate tool for assessing microbial genome quality using machine learning.
1083 bioRxiv 2022.07.11.499243. https://doi.org/10.1101/2022.07.11.499243
1084 Cozannet, M., Borrel, G., Roussel, E., Moalic, Y., Allioux, M., Sanvoisin, A., Toffin, L., Alain,
1085 K., 2020. New Insights into the Ecology and Physiology of Methanomassiliicoccales
1086 from Terrestrial and Aquatic Environments. Microorganisms 9, 30.
1087 https://doi.org/10.3390/microorganisms9010030
1088 Criscuolo, A., Gribaldo, S., 2010. BMGE (Block Mapping and Gathering with Entropy): a new
1089 software for selection of phylogenetic informative regions from multiple sequence
1090 alignments. BMC Evol Biol 10, 210. https://doi.org/10.1186/1471-2148-10-210
1091 Davis, N.M., Proctor, D.M., Holmes, S.P., Relman, D.A., B.J, C., 2018. Simple statistical
1092 identification and removal of contaminant sequences in marker-gene and
1093 metagenomics data. Microbiome 6, 226. https://doi.org/10.1186/s40168-018-0605-2
1094 De Coster, W., D'Hert, S., Schultz, D.T., Cruts, M., Van Broeckhoven, C., 2018. NanoPack:
1095 visualizing and processing long-read sequencing data. Bioinformatics 34, 2666–2669.
1096 https://doi.org/10.1093/bioinformatics/bty149
1097 De La Cuesta-Zuluaga, J., Spector, T.D., Youngblut, N.D., Ley, R.E., 2021. Genomic
1098 Insights into Adaptations of Trimethylamine-Utilizing Methanogens to Diverse Habitats,
1099 Including the Human Gut. mSystems 6, e00939-20.
1100 De La Torre, J.R., Walker, C.B., Ingalls, A.E., Könneke, M., Stahl, D.A., 2008. Cultivation of
1101 a thermophilic ammonia oxidizing archaeon synthesizing crenarchaeol. Environ
1102 Microbiol 10, 810–818. https://doi.org/10.1111/j.1462-2920.2007.01506.x
1103 Dombrowski, N., Williams, T.A., Sun, J., Woodcroft, B.J., Lee, J.-H., Minh, B.Q., Rinke, C.,
1104 Spang, A., 2020. Undinarchaeota illuminate DPANN phylogeny and the impact of gene
1105 transfer on archaeal evolution. Nat Commun 11, 3939. https://doi.org/10.1038/s41467-
1106 020-17408-w
1107 Dreer, M., Pribasnig, T., Hodgskiss, L.H., Luo, Z.-H., Pozaric, F., Schleper, C., 2024. Biofilm
1108 lifestyle as a common trait of ammonia-oxidizing archaea. Biorxiv.
1109 https://doi.org/10.1101/2024.11.18.624116
1110 Eddy, S.R., 2011. Accelerated Profile HMM Searches. PLoS Comput Biol 7, e1002195.
1111 https://doi.org/10.1371/journal.pcbi.1002195
1112 Emms, D.M., Kelly, S., 2019. OrthoFinder: phylogenetic orthology inference for comparative
1113 genomics. Genome Biol 20, 238. https://doi.org/10.1186/s13059-019-1832-y
1114 Fan, Y., Pedersen, O., 2020. Gut microbiota in human metabolic health and disease. Nature
1115 Reviews Microbiology 2020 19:1 19, 55–71. https://doi.org/10.1038/s41579-020-0433-9

1116 Fan, Y., Wu, L., Zhai, B., 2023. The mycobiome: interactions with host and implications in
1117 diseases. Curr Opin Microbiol 75, 102361. https://doi.org/10.1016/J.MIB.2023.102361
1118 Fernandes, A.D., Macklaim, J.M., Linn, T.G., Reid, G., Gloor, G.B., 2013. ANOVA-Like
1119 Differential Expression (ALDEx) Analysis for Mixed Population RNA-Seq. PLoS One 8,
1120 e67019. https://doi.org/10.1371/journal.pone.0067019
1121 Flowers, L., Grice, E.A., 2020. The Skin Microbiota: Balancing Risk and Reward.
1122 https://doi.org/10.1016/j.chom.2020.06.017
1123 Gaci, N., Borrel, G., Tottey, W., O'Toole, P.W., Brugère, J.-F., 2014. Archaea and the human
1124 gut: New beginning of an old story. World J Gastroenterol 20, 16062.
1125 https://doi.org/10.3748/wjg.v20.i43.16062
1126 Garcia, C.J., Pericleous, A., Elsayed, M., Tran, M., Gupta, S., Callaghan, J.D., Stella, N.A.,
1127 Franks, J.M., Thibodeau, P.H., Shanks, R.M.Q., Kadouri, D.E., 2018. Serralysin family
1128 metalloproteases protects Serratia marcescens from predation by the predatory
1129 bacteria Micavibrio aeruginosavorus. Sci Rep 8, 14025. https://doi.org/10.1038/s41598-
1130 018-32330-4
1131 Ghazali, A.-K., Firdaus-Raih, M., Uthaya Kumar, A., Lee, W.-K., Hoh, C.-C., Nathan, S.,
1132 2023. Transitioning from Soil to Host: Comparative Transcriptome Analysis Reveals the
1133 Burkholderia pseudomallei Response to Different Niches. Microbiol Spectr 11.
1134 https://doi.org/10.1128/spectrum.03835-22
1135 Gibbs, G.M., Roelants, K., O'Bryan, M.K., 2008. The CAP Superfamily: Cysteine-Rich
1136 Secretory Proteins, Antigen 5, and Pathogenesis-Related 1 Proteins—Roles in
1137 Reproduction, Cancer, and Immune Defense. Endocr Rev 29, 865–897.
1138 https://doi.org/10.1210/er.2008-0032
1139 Gladwin, M.T., Raat, N.J.H., Shiva, S., Dezfulian, C., Hogg, N., Kim-Shapiro, D.B., Patel,
1140 R.P., 2006. Nitrite as a vascular endocrine nitric oxide reservoir that contributes to
1141 hypoxic signaling, cytoprotection, and vasodilation. American Journal of Physiology-
1142 Heart and Circulatory Physiology 291, H2026–H2035.
1143 https://doi.org/10.1152/ajpheart.00407.2006
1144 Gomaa, E.Z., 2020. Human gut microbiota/microbiome in health and diseases: a review.
1145 Antonie Van Leeuwenhoek 113, 2019–2040. https://doi.org/10.1007/s10482-020-
1146 01474-7
1147 Graham, E.D., Heidelberg, J.F., Tully, B.J., 2018. Potential for primary productivity in a
1148 globally-distributed bacterial phototroph. ISME J 12, 1861–1866.
1149 https://doi.org/10.1038/s41396-018-0091-3
1150 Gremme, G., Steinbiss, S., Kurtz, S., 2013. GenomeTools: A Comprehensive Software
1151 Library for Efficient Processing of Structured Genome Annotations. IEEE/ACM Trans
1152 Comput Biol Bioinform 10, 645–656. https://doi.org/10.1109/TCBB.2013.68
1153 Grice, E.A., Segre, J.A., 2011. The skin microbiome. Nat Rev Microbiol 9, 244–253.
1154 Großkopf, R., Janssen, P.H., Liesack, W., 1998. Diversity and structure of the methanogenic
1155 community in anoxic rice paddy soil microcosms as examined by cultivation and direct
1156 16S rRNA gene sequence retrieval. Appl Environ Microbiol 64, 960–969.
1157 Guindon, S., Dufayard, J.-F., Lefort, V., Anisimova, M., Hordijk, W., Gascuel, O., 2010. New
1158 Algorithms and Methods to Estimate Maximum-Likelihood Phylogenies: Assessing the
1159 Performance of PhyML 3.0. Syst Biol 59, 307–321.
1160 https://doi.org/10.1093/sysbio/syq010
1161 Heidrich, V., Karlovsky, P., Beule, L., 2021. 'SRS' R Package and 'q2-srs' QIIME 2 Plugin:
1162 Normalization of Microbiome Data Using Scaling with Ranked Subsampling (SRS).
1163 Applied Sciences 11, 11473. https://doi.org/10.3390/app112311473

1164 Huerta-Cepas, J., Szklarczyk, D., Heller, D., Hernández-Plaza, A., Forslund, S.K., Cook, H.,
1165 Mende, D.R., Letunic, I., Rattei, T., Jensen, L.J., 2019. eggNOG 5.0: a hierarchical,
1166 functionally and phylogenetically annotated orthology resource based on 5090
1167 organisms and 2502 viruses. Nucleic Acids Res 47, D309–D314.
1168 Hyatt, D., Chen, G.-L., LoCascio, P.F., Land, M.L., Larimer, F.W., Hauser, L.J., 2010.
1169 Prodigal: prokaryotic gene recognition and translation initiation site identification. BMC
1170 Bioinformatics 11, 119. https://doi.org/10.1186/1471-2105-11-119
1171 Jung, M.Y., Kim, J.G., Sinninghe Damsté, J.S., Rijpstra, W.I.C., Madsen, E.L., Kim, S.J.,
1172 Hong, H., Si, O.J., Kerou, M., Schleper, C., Rhee, S.K., 2016. A hydrophobic ammonia-
1173 oxidizing archaeon of the Nitrosocosmicus clade isolated from coal tar-contaminated
1174 sediment. Environ Microbiol Rep 8, 983–992. https://doi.org/10.1111/1758-2229.12477
1175 Kalyaanamoorthy, S., Minh, B.Q., Wong, T.K.F., von Haeseler, A., Jermiin, L.S., 2017.
1176 ModelFinder: fast model selection for accurate phylogenetic estimates. Nat Methods
1177 14, 587–589. https://doi.org/10.1038/nmeth.4285
1178 Katoh, K., Standley, D.M., 2013. MAFFT Multiple Sequence Alignment Software Version 7:
1179 Improvements in Performance and Usability. Mol Biol Evol 30, 772–780.
1180 https://doi.org/10.1093/molbev/mst010
1181 Kim, J.-H., Son, S.-M., Park, H., Kim, B.K., Choi, I.S., Kim, H., Huh, C.S., 2021. Taxonomic
1182 profiling of skin microbiome and correlation with clinical skin parameters in healthy
1183 Koreans. Sci Rep 11, 16269. https://doi.org/10.1038/s41598-021-95734-9
1184 Klein, T., Poghosyan, L., Barclay, J.E., Murrell, J.C., Hutchings, M.I., Lehtovirta-Morley, L.E.,
1185 2022. Cultivation of ammonia-oxidising archaea on solid medium. FEMS Microbiol Lett
1186 369. https://doi.org/10.1093/femsle/fnac029
1187 Klindworth, A., Pruesse, E., Schweer, T., Peplies, J., Quast, C., Horn, M., Glockner, F.O.,
1188 2013. Evaluation of general 16S ribosomal RNA gene PCR primers for classical and
1189 next-generation sequencing-based diversity studies. Nucleic Acids Res 41, e1–e1.
1190 https://doi.org/10.1093/nar/gks808
1191 Kobe, B., 2001. The leucine-rich repeat as a protein recognition motif. Curr Opin Struct Biol
1192 11, 725–732. https://doi.org/10.1016/S0959-440X(01)00266-4
1193 Kolmogorov, M., Bickhart, D.M., Behsaz, B., Gurevich, A., Rayko, M., Shin, S.B., Kuhn, K.,
1194 Yuan, J., Polevikov, E., Smith, T.P.L., Pevzner, P.A., 2020. metaFlye: scalable long-
1195 read metagenome assembly using repeat graphs. Nat Methods 17, 1103–1110.
1196 https://doi.org/10.1038/s41592-020-00971-x
1197 Kong, H.H., 2011. Skin microbiome: genomics-based insights into the diversity and role of
1198 skin microbes. Trends Mol Med 17, 320.
1199 https://doi.org/10.1016/J.MOLMED.2011.01.013
1200 Konstantinidis, K.T., Rosselló-Móra, R., Amann, R., 2017. Uncultivated microbes in need of
1201 their own taxonomy. ISME J 11, 2399–2406. https://doi.org/10.1038/ismej.2017.113
1202 Kozlowski, Jessica A., Kits, K.D., Stein, L.Y., 2016. Comparison of Nitrogen Oxide
1203 Metabolism among Diverse Ammonia-Oxidizing Bacteria. Front Microbiol 7.
1204 https://doi.org/10.3389/fmicb.2016.01090
1205 Kozlowski, Jessica A, Stieglmeier, M., Schleper, C., Klotz, M.G., Stein, L.Y., 2016. Pathways
1206 and key intermediates required for obligate aerobic ammonia-dependent
1207 chemolithotrophy in bacteria and Thaumarchaeota. ISME J 10, 1836–1845.
1208 https://doi.org/10.1038/ismej.2016.2
1209 Kumpitsch, C., Fischmeister, F.P.S., Mahnert, A., Lackner, S., Wilding, M., Sturm, C.,
1210 Springer, A., Madl, T., Holasek, S., Högenauer, C., 2021. Reduced B12 uptake and
1211 increased gastrointestinal formate are associated with archaeome-mediated breath

methane emission in humans. Microbiome 9, 1–18. https://doi.org/10.1186/s40168-021-01130-w

Lane, D., 1991. 16S/23S rRNA sequencing., in: Stackebrandt, E., Goodfellow, M. (Eds.), Nucleic Acid Techniques in Bacterial Systematics. John Wiley & Sons, Chichester, pp. 115–175.

Larsson, A., 2014. AliView: a fast and lightweight alignment viewer and editor for large datasets. Bioinformatics 30, 3276–3278. https://doi.org/10.1093/bioinformatics/btu531

Lee, U.-J., Gwak, J.-H., Choi, S., Jung, M.-Y., Lee, T.K., Ryu, H., Imisi Awala, S., Wanek, W., Wagner, M., Quan, Z.-X., Rhee, S.-K., 2024. " Ca. Nitrosocosmicus" members are the dominant archaea associated with plant rhizospheres. mSphere 9. https://doi.org/10.1128/msphere.00821-24

Lehtovirta-Morley, L.E., Ross, J., Hink, L., Weber, E.B., Gubry-Rangin, C., Thion, C., Prosser, J.I., Nicol, G.W., 2016. Isolation of 'Candidatus Nitrosocosmicus franklandus', a novel ureolytic soil archaeal ammonia oxidiser with tolerance to high ammonia concentration. FEMS Microbiol Ecol 92, 57. https://doi.org/10.1093/FEMSEC/FIW057

Leininger, S., Urich, T., Schloter, M., Schwark, L., Qi, J., Nicol, G.W., Prosser, J.I., Schuster, S.C., Schleper, C., 2006. Archaea predominate among ammonia-oxidizing prokaryotes in soils. Nature 442, 806–809.

Li, H., 2021. New strategies to improve minimap2 alignment accuracy. Bioinformatics 37, 4572–4574. https://doi.org/10.1093/bioinformatics/btab705

Li, M., Kopylova, E., Mao, J., Namkoong, J., Sanders, J., Wu, J., 2024. Microbiome and lipidomic analysis reveal the interplay between skin bacteria and lipids in a cohort study. Front Microbiol 15. https://doi.org/10.3389/fmicb.2024.1383656

Lin, H., Peddada, S. Das, 2020. Analysis of compositions of microbiomes with bias correction. Nat Commun 11, 3514. https://doi.org/10.1038/s41467-020-17041-7

Liu, L., Liu, M., Jiang, Y., Lin, W., Luo, J., 2021. Production and Excretion of Polyamines To Tolerate High Ammonia, a Case Study on Soil Ammonia-Oxidizing Archaeon " Candidatus Nitrosocosmicus agrestis." mSystems 6. https://doi.org/10.1128/MSYSTEMS.01003-20

Lozupone, C., Knight, R., 2005. UniFrac: a New Phylogenetic Method for Comparing Microbial Communities. Appl Environ Microbiol 71, 8228–8235. https://doi.org/10.1128/AEM.71.12.8228-8235.2005

Lu, J., Salzberg, S.L., 2020. Ultrafast and accurate 16S rRNA microbial community analysis using Kraken 2. Microbiome 8, 124. https://doi.org/10.1186/s40168-020-00900-2

Mahnert, A., Blohs, M., Pausan, M.R., Moissl-Eichinger, C., 2018. The human archaeome: methodological pitfalls and knowledge gaps. Emerg Top Life Sci 2.4, 469–482. https://doi.org/10.1042/ETLS20180037

Makarova, K.S., Galperin, M.Y., Koonin, E. V., 2015. Comparative genomic analysis of evolutionarily conserved but functionally uncharacterized membrane proteins in archaea: Prediction of novel components of secretion, membrane remodeling and glycosylation systems. Biochimie 118, 302–312. https://doi.org/10.1016/j.biochi.2015.01.004

Mallick, H., Rahnavard, A., McIver, L.J., Ma, S., Zhang, Y., Nguyen, L.H., Tickle, T.L., Weingart, G., Ren, B., Schwager, E.H., Chatterjee, S., Thompson, K.N., Wilkinson, J.E., Subramanian, A., Lu, Y., Waldron, L., Paulson, J.N., Franzosa, E.A., Bravo, H.C., Huttenhower, C., 2021. Multivariable association discovery in population-scale meta-omics studies. PLoS Comput Biol 17, e1009442. https://doi.org/10.1371/journal.pcbi.1009442

1260 Martino, C., Morton, J.T., Marotz, C.A., Thompson, L.R., Tripathi, A., Knight, R., Zengler, K.,
1261 2019. A Novel Sparse Compositional Technique Reveals Microbial Perturbations.
1262 mSystems 4. https://doi.org/10.1128/mSystems.00016-19
1263 Marullo, S., Coureuil, M., 2014. Arrestins in host-pathogen interactions. Handb Exp
1264 Pharmacol 219, 361–74. https://doi.org/10.1007/978-3-642-41199-1_18
1265 Meulenbroek, E.M., Peron Cane, C., Jala, I., Iwai, S., Moolenaar, G.F., Goosen, N., Pannu,
1266 N.S., 2013. UV damage endonuclease employs a novel dual-dinucleotide flipping
1267 mechanism to recognize different DNA lesions. Nucleic Acids Res 41, 1363–1371.
1268 https://doi.org/10.1093/nar/gks1127
1269 Minh, B.Q., Schmidt, H.A., Chernomor, O., Schrempf, D., Woodhams, M.D., von Haeseler,
1270 A., Lanfear, R., 2020. IQ-TREE 2: New Models and Efficient Methods for Phylogenetic
1271 Inference in the Genomic Era. Mol Biol Evol 37, 1530–1534.
1272 https://doi.org/10.1093/molbev/msaa015
1273 Moissl-Eichinger, C., 2011. Archaea in artificial environments: their presence in global
1274 spacecraft clean rooms and impact on planetary protection. ISME J 5, 209–19.
1275 https://doi.org/10.1038/ismej.2010.124
1276 Moissl-Eichinger, C., Probst, A.J., Birarda, G., Auerbach, A., Koskinen, K., Wolf, P., Holman,
1277 H.-Y.N., 2017. Human age and skin physiology shape diversity and abundance of
1278 Archaea on skin. Sci Rep 7. https://doi.org/10.1038/s41598-017-04197-4
1279 Mondal, A.K., Lata, K., Singh, M., Chatterjee, S., Chauhan, A., Puravankara, S.,
1280 Chattopadhyay, K., 2022. Cryo-EM elucidates mechanism of action of bacterial pore-
1281 forming toxins. Biochimica et Biophysica Acta (BBA) - Biomembranes 1864, 184013.
1282 https://doi.org/10.1016/j.bbamem.2022.184013
1283 Nayfach, S., Páez-Espino, D., Call, L., Low, S.J., Sberro, H., Ivanova, N.N., Proal, A.D.,
1284 Fischbach, M.A., Bhatt, A.S., Hugenholtz, P., Kyrpides, N.C., 2021. Metagenomic
1285 compendium of 189,680 DNA viruses from the human gut microbiome. Nature
1286 Microbiology 2021 6:7 6, 960–970. https://doi.org/10.1038/s41564-021-00928-6
1287 Nicol, G.W., Leininger, S., Schleper, C., Prosser, J.I., 2008. The influence of soil pH on the
1288 diversity, abundance and transcriptional activity of ammonia oxidizing archaea and
1289 bacteria. Environ Microbiol 10, 2966–2978. https://doi.org/10.1111/j.1462-
1290 2920.2008.01701.x
1291 Ochsenreiter, T., Selezi, D., Quaiser, A., Bonch-Osmolovskaya, L., Schleper, C., 2003.
1292 Diversity and abundance of Crenarchaeota in terrestrial habitats studied by 16S RNA
1293 surveys and real time PCR. Environ Microbiol 5, 787–797.
1294 https://doi.org/10.1046/j.1462-2920.2003.00476.x
1295 Oh, J., Byrd, A.L., Park, M., Kong, H.H., Segre, J.A., 2016. Temporal Stability of the Human
1296 Skin Microbiome. Cell 165, 854–866. https://doi.org/10.1016/j.cell.2016.04.008
1297 Olm, M.R., Brown, C.T., Brooks, B., Banfield, J.F., 2017. DRep: A tool for fast and accurate
1298 genomic comparisons that enables improved genome recovery from metagenomes
1299 through de-replication. ISME Journal 11, 2864–2868.
1300 https://doi.org/10.1038/ismej.2017.126
1301 Parks, D.H., Chuvochina, M., Chaumeil, P.-A., Rinke, C., Mussig, A.J., Hugenholtz, P., 2020.
1302 A complete domain-to-species taxonomy for Bacteria and Archaea. Nat Biotechnol 38,
1303 1079–1086. https://doi.org/10.1038/s41587-020-0501-8
1304 Parks, D.H., Chuvochina, M., Rinke, C., Mussig, A.J., Chaumeil, P.A., Hugenholtz, P., 2022.
1305 GTDB: an ongoing census of bacterial and archaeal diversity through a phylogenetically
1306 consistent, rank normalized and complete genome-based taxonomy. Nucleic Acids Res
1307 50, D785–D794. https://doi.org/10.1093/NAR/GKAB776

1308 Pausan, M.R., Csorba, C., Singer, G., Till, H., Schöpf, V., Santigli, E., Klug, B., Högenauer,
1309 C., Blohs, M., Moissl-Eichinger, C., 2019. Exploring the Archaeome: Detection of
1310 Archaeal Signatures in the Human Body. Front Microbiol 10.
1311 https://doi.org/10.3389/fmicb.2019.02796
1312 Pester, M., Rattei, T., Flechl, S., Gröngröft, A., Richter, A., Overmann, J., Reinhold-Hurek,
1313 B., Loy, A., Wagner, M., 2012. amoA-based consensus phylogeny of ammonia-
1314 oxidizing archaea and deep sequencing of amoA genes from soils of four different
1315 geographic regions. Environ Microbiol 14, 525–539. https://doi.org/10.1111/j.1462-
1316 2920.2011.02666.x
1317 Price, M.N., Dehal, P.S., Arkin, A.P., 2010. FastTree 2 - Approximately maximum-likelihood
1318 trees for large alignments. PLoS One 5. https://doi.org/10.1371/journal.pone.0009490
1319 Probst, A.J., Auerbach, A.K., Moissl-Eichinger, C., 2013. Archaea on human skin. PLoS One
1320 8, e65388. https://doi.org/10.1371/journal.pone.0065388
1321 Pruesse, E., Peplies, J., Glöckner, F.O., 2012. SINA: accurate high-throughput multiple
1322 sequence alignment of ribosomal RNA genes. Bioinformatics 28, 1823–1829.
1323 Rayan, G.M., Flournoy, D.J., 1987. Microbiologic flora of human fingernails. J Hand Surg Am
1324 12, 605–607. https://doi.org/10.1016/S0363-5023(87)80217-4
1325 Reyes, C., Hodgskiss, L.H., Baars, O., Kerou, M., Bayer, B., Schleper, C., Kraemer, S.M.,
1326 2020. Copper limiting threshold in the terrestrial ammonia oxidizing archaeon
1327 Nitrososphaera viennensis. Res Microbiol 171, 134–142.
1328 https://doi.org/10.1016/J.RESMIC.2020.01.003
1329 Rinke, C., Chuvochina, M., Mussig, A.J., Chaumeil, P.-A., Davín, A.A., Waite, D.W.,
1330 Whitman, W.B., Parks, D.H., Hugenholtz, P., 2021. A standardized archaeal taxonomy
1331 for the Genome Taxonomy Database. Nat Microbiol 1–14.
1332 Rinke, C., Schwientek, P., Sczyrba, A., Ivanova, N.N., Anderson, I.J., Cheng, J.-F., Darling,
1333 A., Malfatti, S., Swan, B.K., Gies, E.A., Dodsworth, J.A., Hedlund, B.P., Tsiamis, G.,
1334 Sievert, S.M., Liu, W.-T., Eisen, J.A., Hallam, S.J., Kyrpides, N.C., Stepanauskas, R.,
1335 Rubin, E.M., Hugenholtz, P., Woyke, T., 2013. Insights into the phylogeny and coding
1336 potential of microbial dark matter. Nature 499, 431–437.
1337 https://doi.org/10.1038/nature12352
1338 Robeson, M.S., O'Rourke, D.R., Kaehler, B.D., Ziemski, M., Dillon, M.R., Foster, J.T.,
1339 Bokulich, N.A., 2021. RESCRIPt: Reproducible sequence taxonomy reference
1340 database management. PLoS Comput Biol 17, e1009581.
1341 https://doi.org/10.1371/journal.pcbi.1009581
1342 Ross, A.A., Doxey, A.C., Neufeld, J.D., 2017. The Skin Microbiome of Cohabiting Couples.
1343 mSystems 2. https://doi.org/10.1128/mSystems.00043-17
1344 Saier, M.H., Reddy, V.S., Tsu, B. V., Ahmed, M.S., Li, C., Moreno-Hagelsieb, G., 2016. The
1345 Transporter Classification Database (TCDB): recent advances. Nucleic Acids Res 44,
1346 D372–D379. https://doi.org/10.1093/nar/gkv1103
1347 Soto, W., Nishiguchi, M.K., 2021. Environmental Stress Selects for Innovations That Drive
1348 Vibrio Symbiont Diversity. Front Ecol Evol 9. https://doi.org/10.3389/fevo.2021.616973
1349 Steinegger, M., Söding, J., 2017. MMseqs2 enables sensitive protein sequence searching
1350 for the analysis of massive data sets. Nat Biotechnol 35, 1026–1028.
1351 https://doi.org/10.1038/nbt.3988
1352 Sun, Y., Liu, Y., Pan, J., Wang, F., Li, M., 2019. Perspectives on Cultivation Strategies of
1353 Archaea. Microb Ecol. https://doi.org/10.1007/s00248-019-01422-7

1354 Suschek, C. V., Opländer, C., van Faassen, E.E., 2010. Non-enzymatic NO production in
1355 human skin: Effect of UVA on cutaneous NO stores. Nitric Oxide 22, 120–135.
1356 https://doi.org/10.1016/j.niox.2009.10.006
1357 Taylor, D.L., Bruns, T.D., 1999. Community structure of ectomycorrhizal fungi in a *Pinus*
1358 *muricata* forest: minimal overlap between the mature forest and resistant propagule
1359 communities. Mol Ecol 8, 1837–1850. https://doi.org/10.1046/j.1365-294x.1999.00773.x
1360 Tourna, M., Freitag, T.E., Nicol, G.W., Prosser, J.I., 2008. Growth, activity and temperature
1361 responses of ammonia-oxidizing archaea and bacteria in soil microcosms. Environ
1362 Microbiol 10, 1357–1364. https://doi.org/10.1111/j.1462-2920.2007.01563.x
1363 Tourna, M., Stieglmeier, M., Spang, A., Könneke, M., Schintlmeister, A., Urich, T., Engel, M.,
1364 Schloter, M., Wagner, M., Richter, A., Schleper, C., 2011. Nitrososphaera viennensis,
1365 an ammonia oxidizing archaeon from soil. Proc Natl Acad Sci U S A 108, 8420–8425.
1366 https://doi.org/10.1073/PNAS.1013488108/SUPPL_FILE/PNAS.201013488SI.PDF
1367 Umbach, A.K., Stegelmeier, A.A., Neufeld, J.D., 2021. Archaea Are Rare and Uncommon
1368 Members of the Mammalian Skin Microbiome. mSystems 6.
1369 https://doi.org/10.1128/MSYSTEMS.00642-21/ASSET/1CFB65AC-B6A0-4252-8E75-
1370 629C6EA38AC1/ASSETS/IMAGES/LARGE/MSYSTEMS.00642-21-F004.JPG
1371 Untereiner, W.A., Naveau, F.A., 1999. Molecular systematics of the Herpotrichiellaceae with
1372 an assessment of the phylogenetic positions of Exophiala dermatitidis and Phialophora
1373 americana. Mycologia 91, 67–83. https://doi.org/10.1080/00275514.1999.12060994
1374 Usuda, D., Higashikawa, T., Hotchi, Y., Usami, K., Shimozawa, S., Tokunaga, S., Osugi, I.,
1375 Katou, R., Ito, S., Yoshizawa, T., Asako, S., Mishima, K., Kondo, A., Mizuno, K.,
1376 Takami, H., Komatsu, T., Oba, J., Nomura, T., Sugita, M., 2021. Exophiala dermatitidis.
1377 World J Clin Cases 9, 7963–7972. https://doi.org/10.12998/wjcc.v9.i27.7963
1378 Vallenet, D., Calteau, A., Dubois, M., Amours, P., Bazin, A., Beuvin, M., Burlot, L., Bussell,
1379 X., Fouteau, S., Gautreau, G., Lajus, A., Langlois, J., Planel, R., Roche, D., Rollin, J.,
1380 Rouy, Z., Sabatet, V., Médigue, C., 2020. MicroScope: an integrated platform for the
1381 annotation and exploration of microbial gene functions through genomic, pangenomic
1382 and metabolic comparative analysis. Nucleic Acids Res 48, D579–D589.
1383 https://doi.org/10.1093/NAR/GKZ926
1384 van Ulsen, P., Zinner, K.M., Jong, W.S.P., Luirink, J., 2018. On display: autotransporter
1385 secretion and application. FEMS Microbiol Lett 365.
1386 https://doi.org/10.1093/femsle/fny165
1387 Walters, W.A., Caporaso, J.G., Lauber, C.L., Berg-Lyons, D., Fierer, N., Knight, R., 2011.
1388 PrimerProspector: de novo design and taxonomic analysis of barcoded polymerase
1389 chain reaction primers. Bioinformatics 27, 1159–1161.
1390 Wang, H., Bagnoud, A., Ponce-Toledo, R.I., Kerou, M., Weil, M., Schleper, C., Urich, T.,
1391 2021. Linking 16S rRNA Gene Classification to *amoA* Gene Taxonomy Reveals
1392 Environmental Distribution of Ammonia-Oxidizing Archaeal Clades in Peatland Soils.
1393 mSystems 6. https://doi.org/10.1128/mSystems.00546-21
1394 Wood, D.E., Lu, J., Langmead, B., 2019. Improved metagenomic analysis with Kraken 2.
1395 Genome Biol 20, 257. https://doi.org/10.1186/s13059-019-1891-0
1396 Yeats, C., Bentley, S., Bateman, A., 2003. New Knowledge from Old: In silico discovery of
1397 novel protein domains in Streptomyces coelicolor. BMC Microbiol 3, 3.
1398 https://doi.org/10.1186/1471-2180-3-3
1399 Zhang, H., Yohe, T., Huang, L., Entwistle, S., Wu, P., Yang, Z., Busk, P.K., Xu, Y., Yin, Y.,
1400 2018. dbCAN2: a meta server for automated carbohydrate-active enzyme annotation.
1401 Nucleic Acids Res 46, W95–W101. https://doi.org/10.1093/nar/gky418

1402

1403

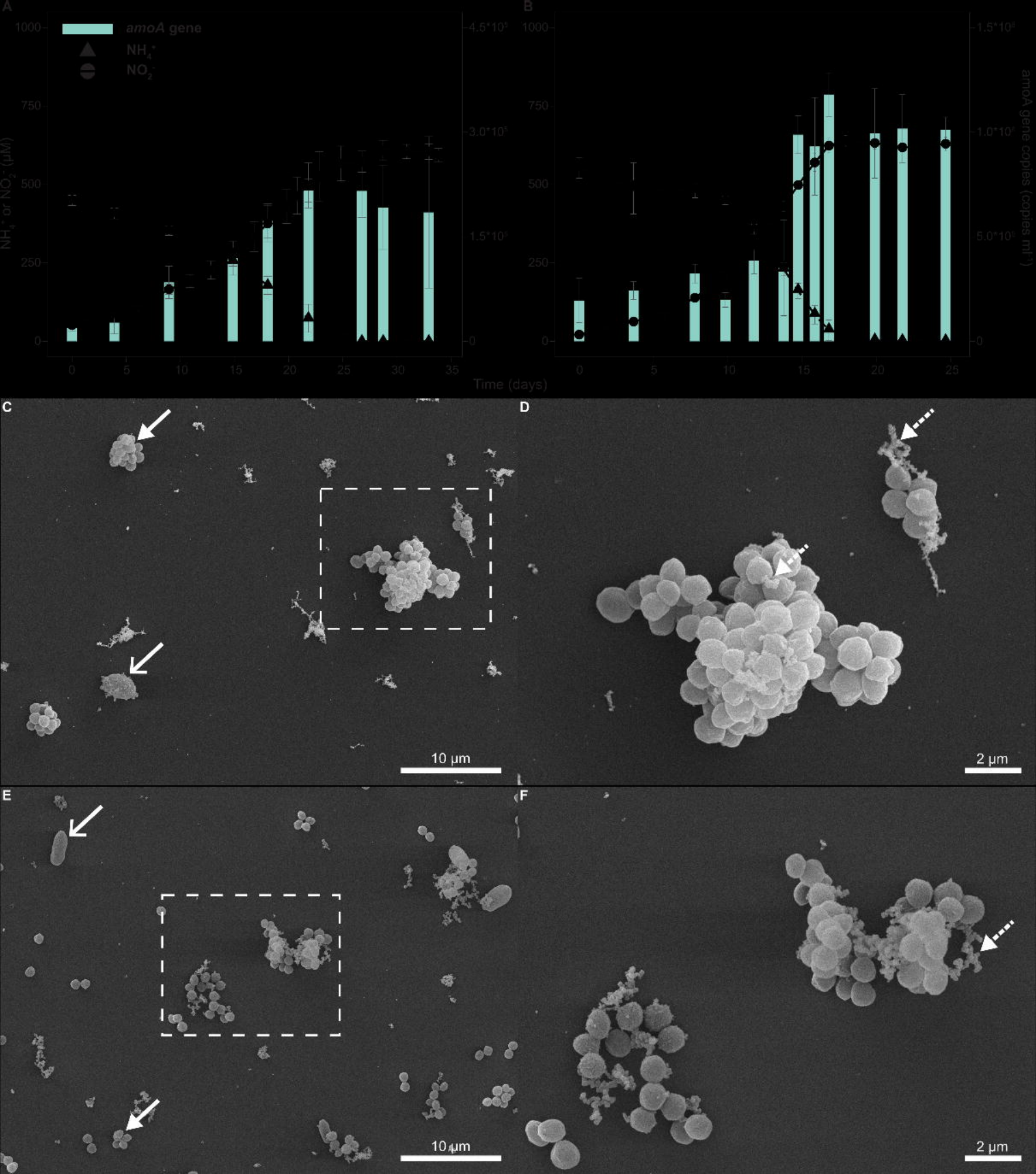
A
B
amoA gene
NH4+
NO2-
NH4+ or NO2- (µM)
amoA gene copies (copies ml-1)
Time (days)
C
D
E
F
10 µm
2 µm
10 µm
2 µm

A

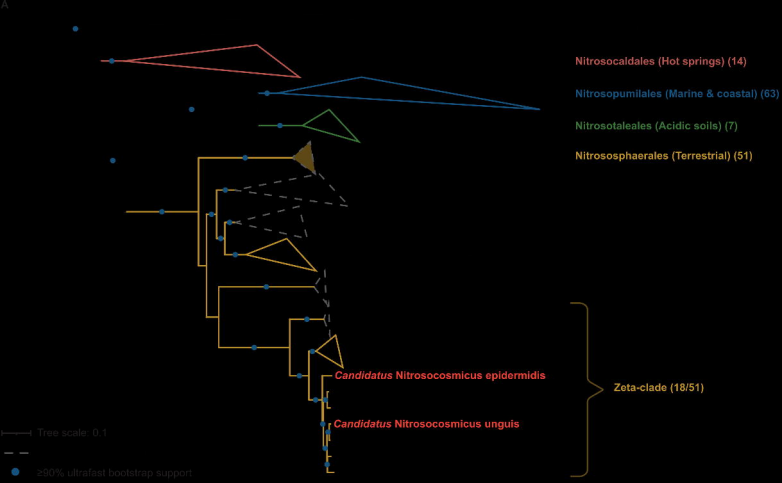

B

Domain desctiption	Domain ID	NS-ζ							NS-α		NT-α
		N.arc	N.frank	N.oleo	N.hydr	N.agr	**N.ung**	**N.epid**	N.vie	N.ever	N.deve
Sialidases		2	7	13	9	9	4	5	7	11	4
Putative Lipases		5	6	14	7	9	13	12	5	6	1
		2	4	3	3	2	1	5	1	3	0
		2	2	2	4	2	1	2	0	1	0
		3	7	15	11	5	14	4	2	6	1
		1	1	1	1	1	1	2	0	1	0
		1	1	1	0	1	3	2	0	0	0
Adhesion-related and surface recognition-related domains		1	1	1	1	0	1	1	0	0	0
		12	14	23	20	19	15	13	6	9	9
		5	5	5	5	6	6	2	0	0	4
		2	3	2	4	3	3	2	1	1	0
		2	2	2	2	2	2	2	2	1	1
		0	0	1	1	0	1	0	0	0	0
		1	1	1	1	1	1	1	4	2	3
		2	8	4	5	7	4	3	18	20	21
		1	1	1	4	1	1	1	3	3	0
		1	1	1	1	1	1	1	4	2	3
		0	0	0	0	0	1	0	1	0	12
Virulence-associated and interaction-associated domains		0	3	0	0	2	3	4	1	1	0
		0	4	2	2	4	4	6	2	2	1
		0	1	4	5	0	7	1	0	0	0
		1	1	1	1	1	1	1	0	0	0
Peptidases		4	3	4	3	4	4	5	2	2	4
		2	4	3	4	3	4	5	1	1	2
		1	1	1	1	1	1	1	2	1	4
		4	4	4	5	3	4	4	4	4	3
		0	1	0	1	0	1	1	0	0	0
		2	5	4	4	3	4	5	1	2	2
		1	1	1	2	1	1	1	1	1	0
		1	1	1	1	1	1	1	0	1	0
		2	5	5	5	2	5	2	1	2	1
		2	1	2	1	1	5	3	0	0	0
		1	4	3	6	5	3	0	0	0	0
		1	1	2	2	1	1	1	1	1	1
		1	2	2	1	2	2	3	3	3	2
		1	1	1	1	1	1	1	2	1	4

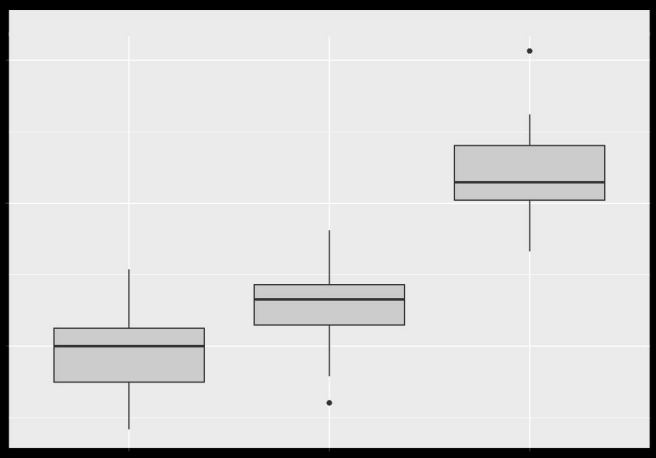

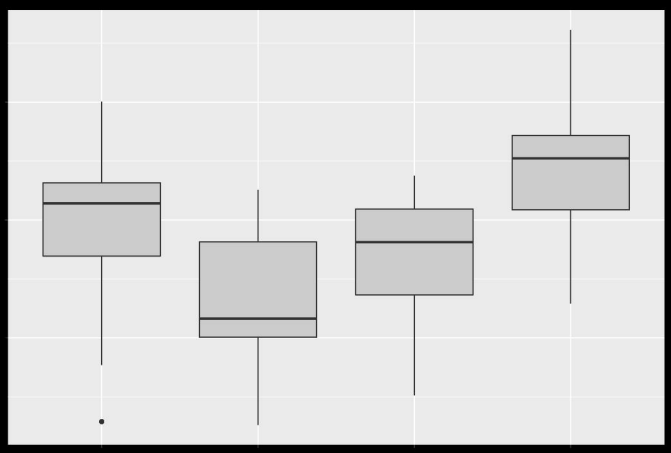

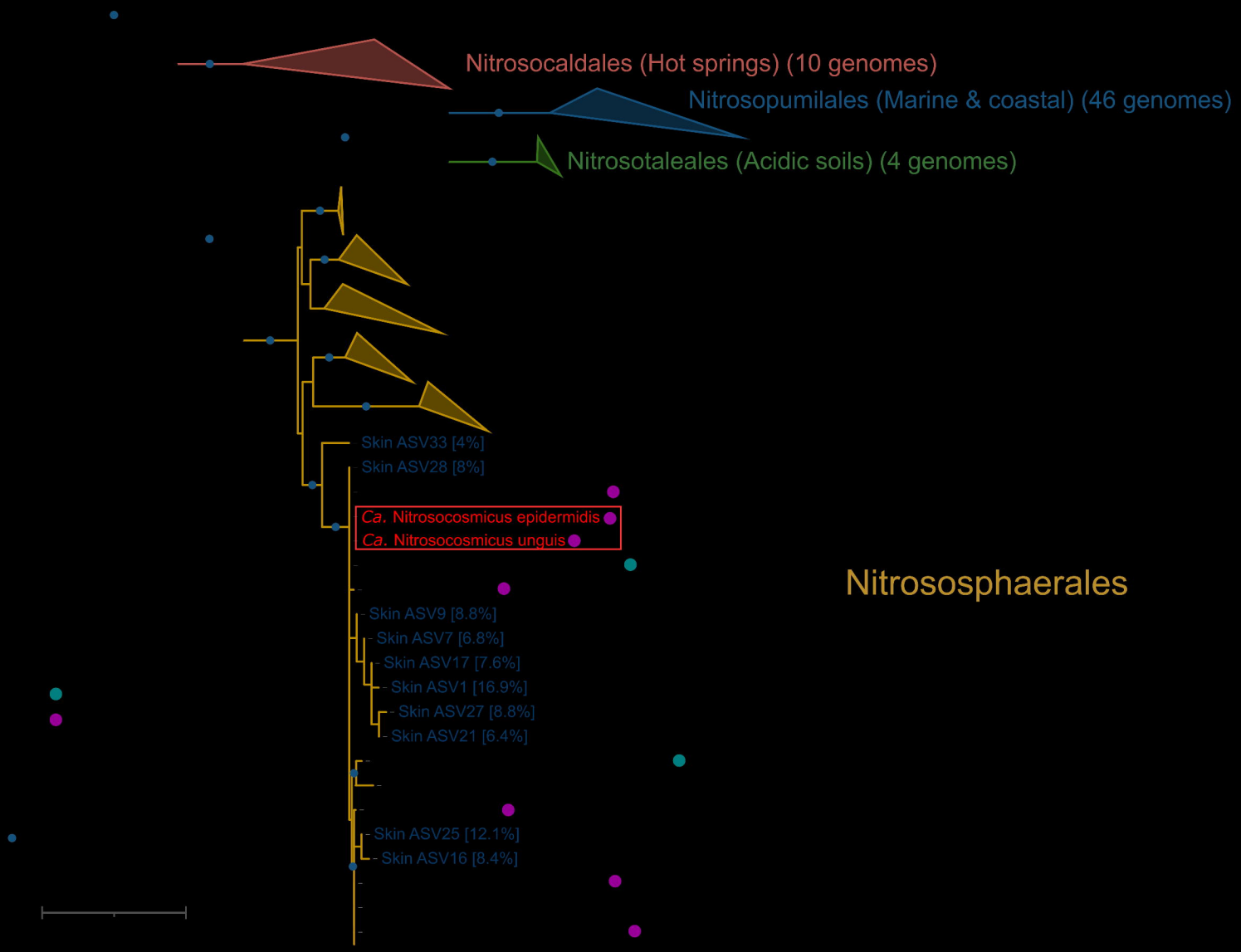
Nitrosocaldales (Hot springs) (10 genomes)
Nitrosopumilales (Marine & coastal) (46 genomes)
Nitrosotaleales (Acidic soils) (4 genomes)
Skin ASV33 [4%]
Skin ASV28 [8%]
Ca. Nitrosocosmicus epidermidis
Ca. Nitrosocosmicus unguis
Nitrososphaerales
Skin ASV9 [8.8%]
Skin ASV7 [6.8%]
Skin ASV17 [7.6%]
Skin ASV1 [16.9%]
Skin ASV27 [8.8%]
Skin ASV21 [6.4%]
Skin ASV25 [12.1%]
Skin ASV16 [8.4%]

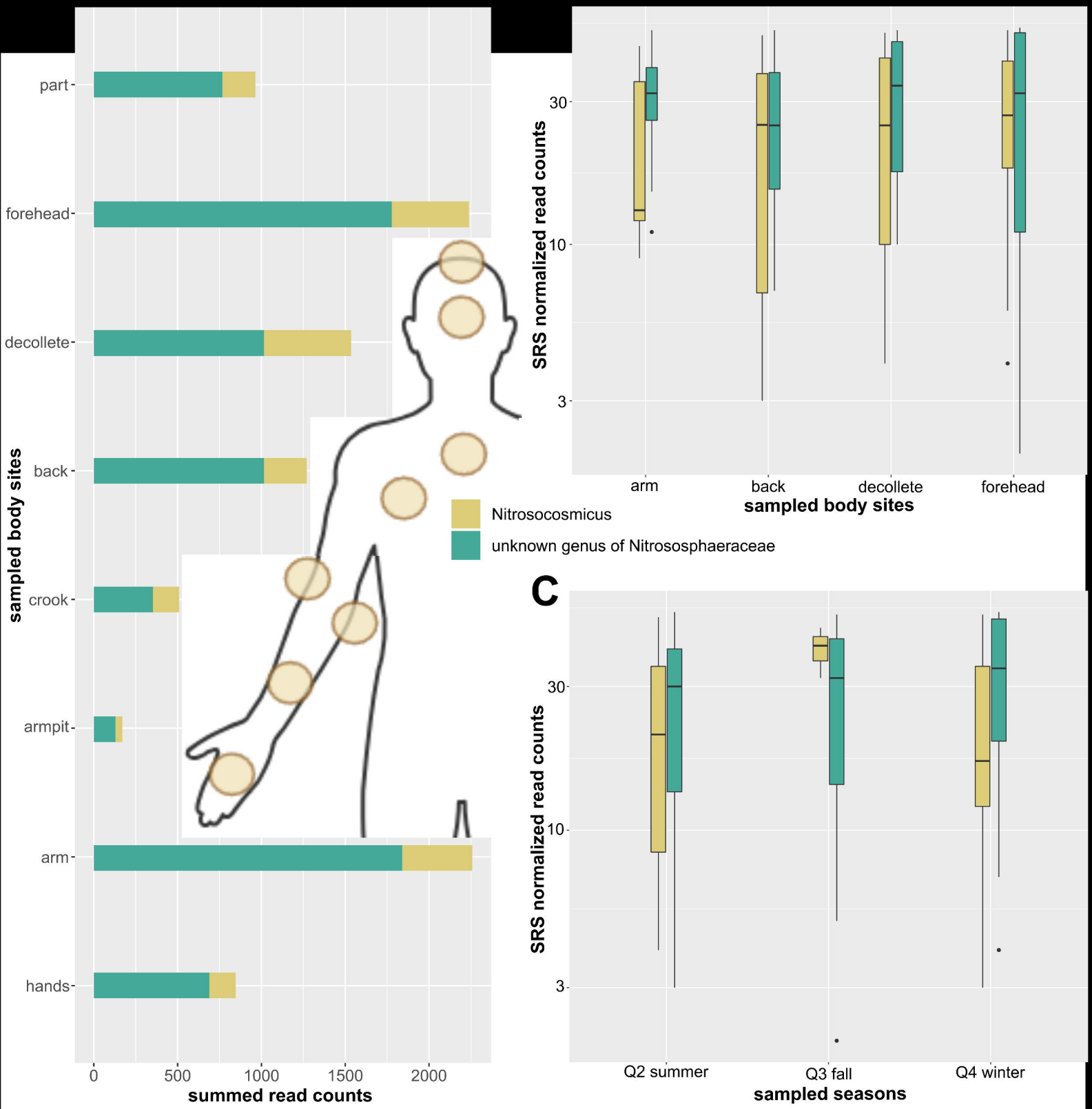
part
forehead
decollete
back
crook
armpit
arm
hands
sampled body sites
0
500
1000
1500
2000
summed read counts
Nitrosocosmicus
unknown genus of Nitrososphaeraceae
SRS normalized read counts
30
10
3
arm
back
decollete
forehead
sampled body sites
C
SRS normalized read counts
30
10
3
Q2 summer
Q3 fall
Q4 winter
sampled seasons

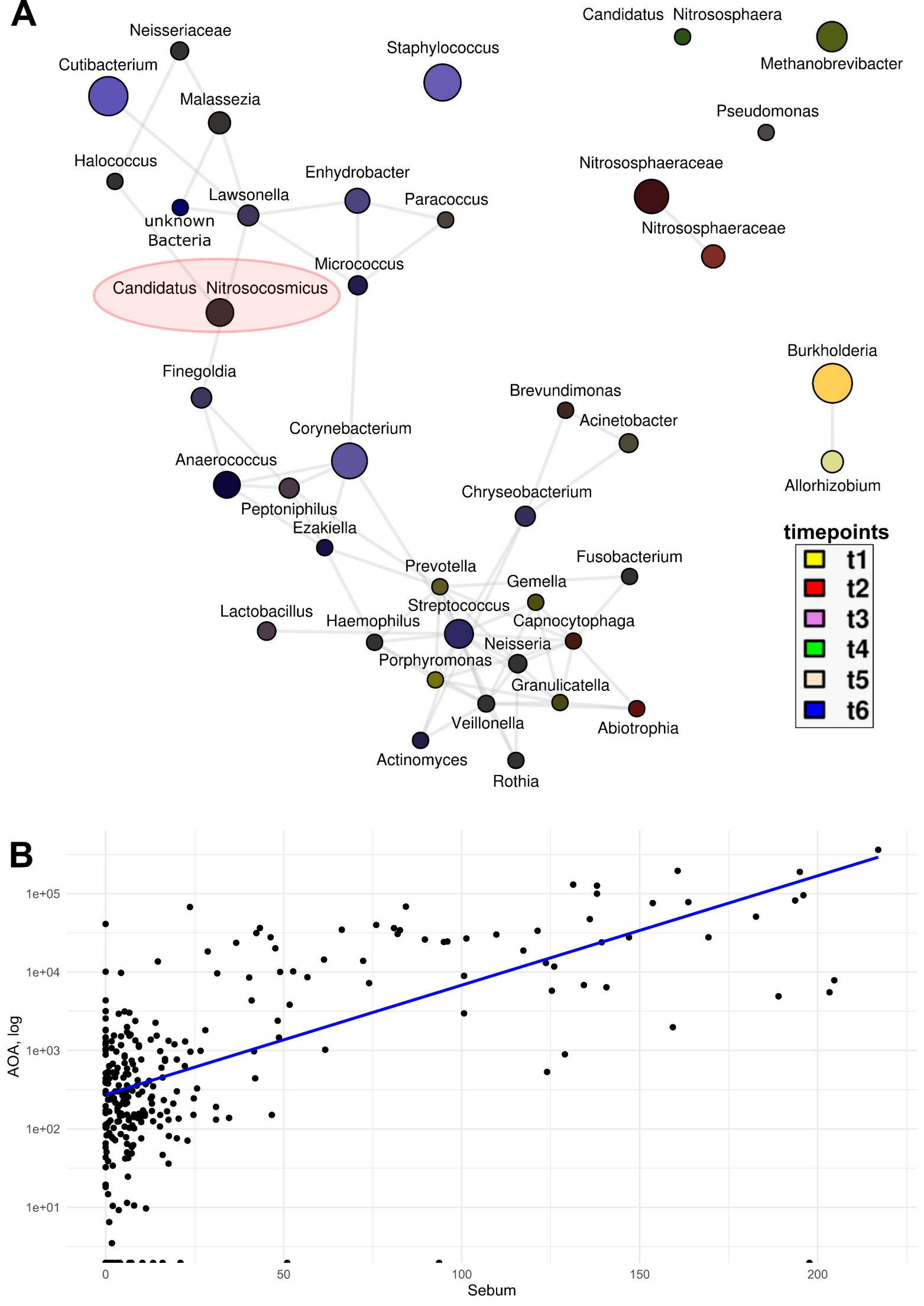
A
Neisseriaceae
Cutibacterium
Malassezia
Staphylococcus
Candidatus Nitrososphaera
Methanobrevibacter
Pseudomonas
Halococcus
Enhydrobacter
Lawsonella
Paracoccus
unknown Bacteria
Nitrososphaeraceae
Nitrososphaeraceae
Micrococcus
Candidatus Nitrosocosmicus
Burkholderia
Finegoldia
Brevundimonas
Acinetobacter
Corynebacterium
Anaerococcus
Allorhizobium
Chryseobacterium
Peptoniphilus
Ezakiella
timepoints
t1
t2
t3
t4
t5
t6
Fusobacterium
Prevotella
Gemella
Streptococcus
Lactobacillus
Haemophilus
Capnocytophaga
Neisseria
Porphyromonas
Granulicatella
Veillonella
Abiotrophia
Actinomyces
Rothia
B
1e+05
1e+04
1e+03
1e+02
1e+01
AOA, log
0
50
100
150
200
Sebum